

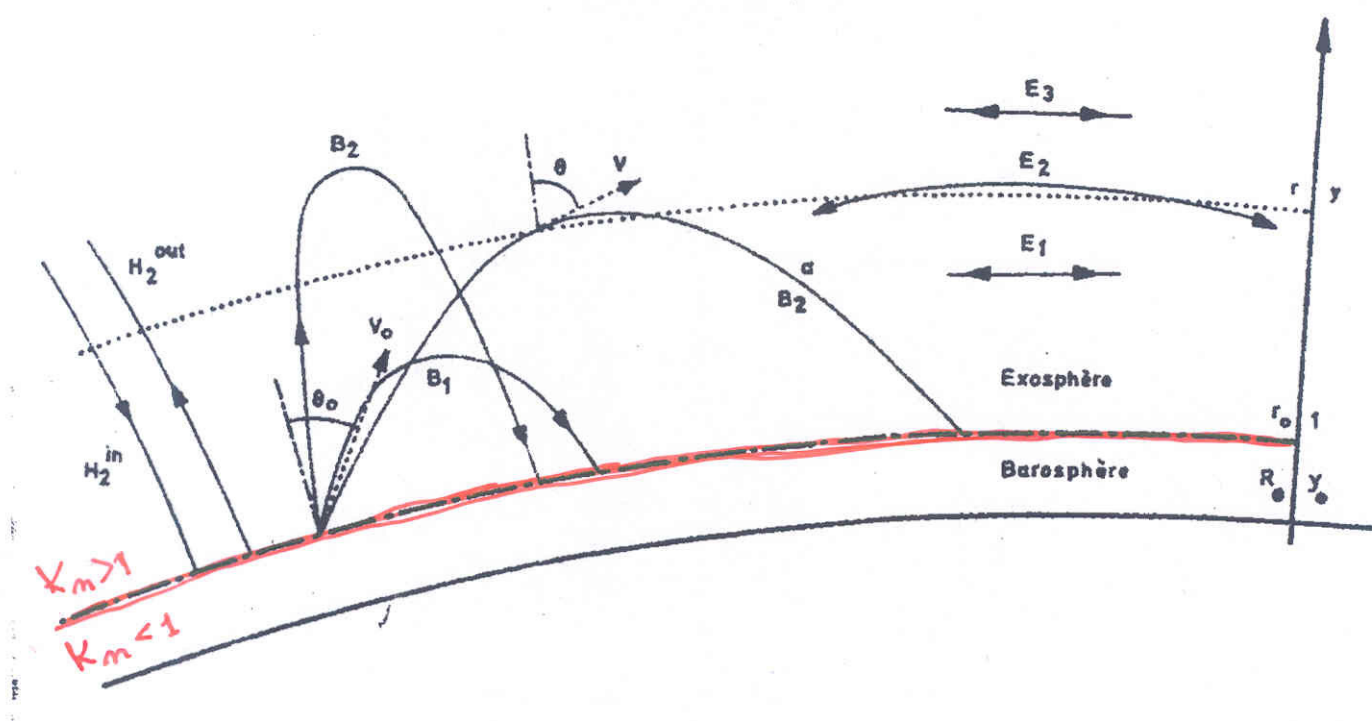
Hydrodynamic and kinetic models of the solar and polar winds (Part 2)

J. LEMAIRE
IASB & CSR. UCL

- SW hydrodynamic solutions become collisionless at exobase where Knudsen number (Kn) becomes equal to unity.
This occurs below 5 solar radii, before the critical sonic (saddle) point in hydrodynamic models.

(Copies of a review article describing the early historical developments of solar and polar wind modelling are available. It contains the hydrodynamic transport equations equations that any SW and PW models does have to satisfy, including the kinetic models discussed in todays lecture).

- Kinetic solutions determine the Velocity Distribution Function (VDF) above exobase
 - Exospheric models : Zero-order kinetic models (no collisions)
 - Fokker-Planck solutions for VDF: First-order kinetic models of SW & PW taking in account the effects of local collisions
 - Monte-Carlo simulations of ions escaping from solar corona and from polar ionosphere also simulate Coulomb collisions
 -



v_o : critical escape velocity of particle
of mass m and charge Ze

$$\frac{1}{2} m v_o^2 - G M_S m / r_o + Ze \Delta\Phi_E = 0$$

Neutral atom: $Z = 0$

$$v_o = (2 G M_S / r_o)^{1/2} = 617 \text{ km/s} (R_S / r_o)^{1/2}$$

Charged particle :

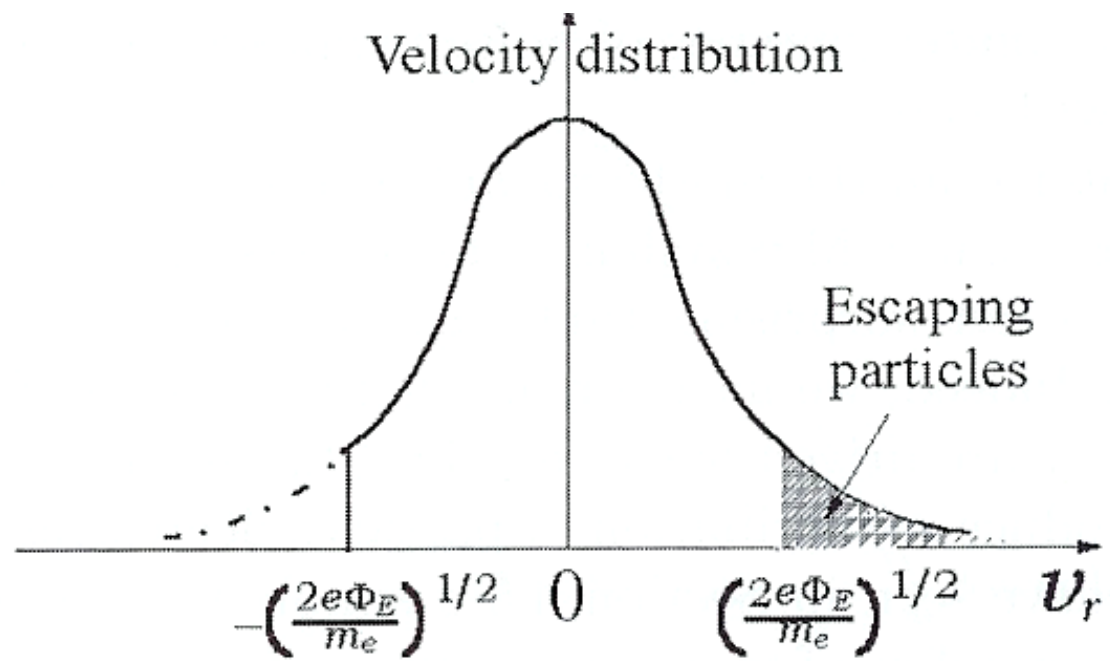
$$v_o = (2 G M_S / r_o - 2 Ze \Delta\Phi_E / m)^{1/2}$$

When $Z > 0$ and $\Delta\Phi_E > 0 \Rightarrow v_o$ is reduced (for protons)

When $Z < 0$ and $\Delta\Phi_E > 0 \Rightarrow v_o$ is increased (for electrons)

- for electrons the electrostatic potential is much more important than the gravitational one (: smallness of m_e)!
- electrons have a large thermal velocity : thus there are many of them with $v > v_o$.
They can escape/evaporate from the level where $Kn = 1$ (exobase). 4

Assume truncated VDF of electrons at exobase : where $\text{Kn} = 1$



Jeans escape flux

Assumptions : no collisions beyond the exobase altitude;
 no magnetic field or a radial B-field distribution;
 conservation of total energy & first adiabatic invariant of charged particles;
 no incoming particles; only particles on escaping, trapped and ballistic orbits;
 truncated Maxwellian VDF at exobase (or other VDF...)

$$F_J(v > v_o) = 2 \pi \int_{v_o}^{\infty} v^3 dv \int_0^{\theta_M} \sin \theta \cos \theta f(v, \theta) d\theta$$

$$\begin{aligned} f(v, r_o) &= n_o (m / 2\pi kT)^{3/2} \exp(-mv^2/2kT) \dots \text{for } v > -v_o \\ &= 0 \quad \dots \dots \dots \dots \dots \dots \text{for } v < -v_o \end{aligned}$$

$$F_J = \frac{1}{4} n_o c_o [1 + \lambda_o] \exp(-\lambda_o)$$

$$c_o = (8 k T / \pi m)^{1/2}$$

$$\lambda_o = m v_o^2 / 2 kT = G M_S m / r_o kT - Z e \Delta \Phi_E / kT$$

When $\Delta\Phi_E = - (m_p - m_e) \Delta\Phi_g / 2 e$ (150 Volts)
& $T_e = T_p \Rightarrow \lambda_{o,p} = \lambda_{o,e}$

$$\frac{F_{J,e}}{F_{J,p}} = \frac{n_{o,e} T_e^{1/2} (1 + \lambda_{o,e}) \exp(-\lambda_{o,e})}{n_{o,p} T_p^{1/2} (1 + \lambda_{o,p}) \exp(-\lambda_{o,p})} (m_p / m_e)^{1/2} \approx 42$$

The flux of electrons evaporating from the corona 42 times larger than escape flux of protons ...

... unless the electrostatic potential difference is larger than the PR electrostatic: 150 Volts

What should be the electrostatic potential difference required to reduce the escape flux of electrons and to balance the flux of protons?

$$F_{J,e} = F_{J,p}$$

$$(1 + \lambda_{o,e}) \exp(-\lambda_{o,e}) (T_e / m_e)^{1/2} = (T_p / m_p)^{1/2} \Rightarrow \lambda_{o,e} = 5.6$$

$$T_e = 1.4 \text{ MK} \Rightarrow \Delta\Phi_E = 617 \text{ Volts}$$

What is the velocity of protons at infinity : v_∞ ?

$$\frac{1}{2} m_p (v_\infty^2 - v_0^2) = -G M_s m_p / r_0 + e \Delta\Phi_E = 317 \text{ eV}$$

... for $v_0 > 0 \Rightarrow v_\infty > 270 \text{ km/s}$

... observed slow SW velocity at 1AU = 300 – 400 km/s

... fast SW ($> 800 \text{ km/s}$) requires $\Delta\Phi_E > 3300 \text{ Volts}$ instead of 150 Volts^8

The moments of f

Number density [m^{-3}]

$$n(\vec{r}) = \int_{-\infty}^{\infty} f(\vec{r}, \vec{v}) d\vec{v}$$

Particle flux [$\text{m}^{-2} \text{s}^{-1}$]

$$\vec{F}(\vec{r}) = \int_{-\infty}^{\infty} f(\vec{r}, \vec{v}) \vec{v} d\vec{v}$$

Bulk velocity [m s^{-1}]

$$\vec{u}(\vec{r}) = \frac{\vec{F}(\vec{r})}{n(\vec{r})}$$

Pressure [Pa]

$$\bar{P}(\vec{r}) = m \int_{-\infty}^{\infty} f(\vec{r}, \vec{v}) (\vec{v} - \vec{u})(\vec{v} - \vec{u}) d\vec{v}$$

Temperature [K]

$$T(\vec{r}) = \frac{m}{3k n(\vec{r})} \int_{-\infty}^{\infty} f(\vec{r}, \vec{v}) |\vec{v} - \vec{u}|^2 d\vec{v}$$

Energy flux [$\text{J m}^{-2} \text{s}^{-1}$]

$$\vec{E}(\vec{r}) = \frac{m}{2} \int_{-\infty}^{\infty} f(\vec{r}, \vec{v}) |\vec{v} - \vec{u}|^2 (\vec{v} - \vec{u}) d\vec{v}$$

For a given $f(v)$ at exobase all these moments of the VDFs are definite integrals which can be calculated analytically or numerically; they are functions of r & $\Phi_E(r)$

The quasi-neutrality equation [: $n_p(r; \Phi_E) = n_e(r, \Phi_E)$]
solved iteratively to determine
electrostatic potential at all altitudes : $\Phi_E(r)$

This electric potential is then used in the analytic expressions of the moments of the VDF to evaluate their values at all altitudes in the exosphere.

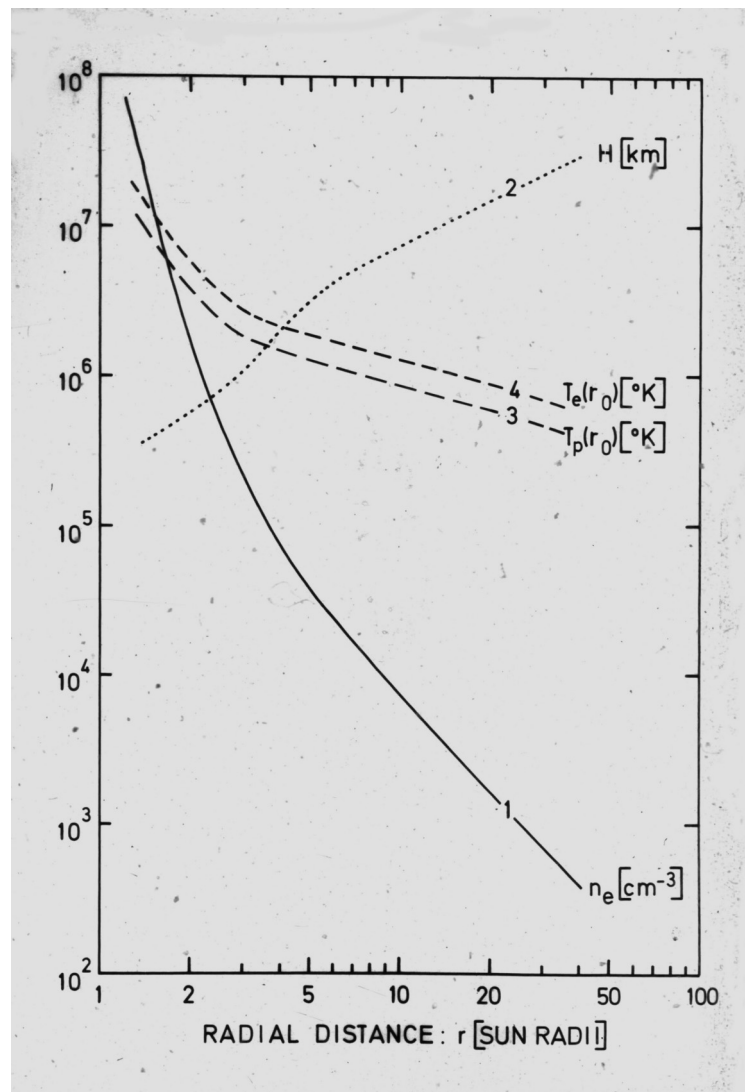
In this is the way one can determine the radial distributions of the solar wind density, bulk velocity, parallel & perpendicular pressure components, parallel and perpendicular temperatures, heat flux of the electrons and protons, etc... without integrating numerically non linear differential equations (hydrodynamical transport equations

Note: that all these moments satisfy, however, the hierarchy (untruncated set) of transport equations which are derived from the collisionless Boltzmann equation or Liouville's equation.

$$\frac{\partial f_s}{\partial t} + \mathbf{v}_s \cdot \nabla f_s + \left[\mathbf{G} + \frac{e_s}{m_s} \left(\mathbf{E} + \frac{1}{c} \mathbf{v}_s \times \mathbf{B} \right) \right] \cdot \nabla_{\mathbf{v}_s} f_s = \frac{\delta f_s}{\delta t} \quad (2.1)$$

$$\mathbf{c}_s = \mathbf{v}_s - \mathbf{u}_s \quad (2.2)$$

where \mathbf{u}_s is the average species velocity, defined below. In terms of the random velocity, Equation (2.1) becomes



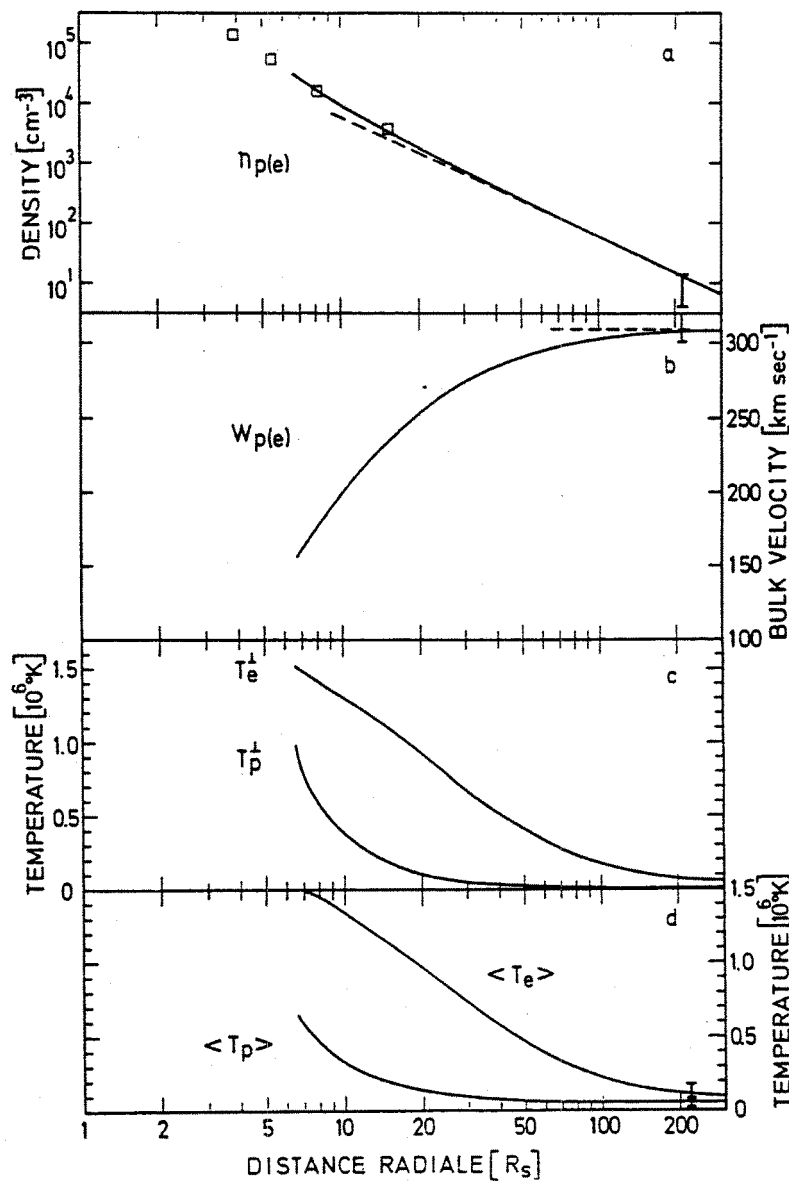


TABLE 2. Solar Wind Properties at 1 AU

Models	$w, \text{ km sec}^{-1}$	$n, \text{ cm}^{-3}$	$\langle T_e \rangle, 10^4 \text{ }^\circ\text{K}$	$\langle T_p \rangle, 10^4 \text{ }^\circ\text{K}$	$T_{e\parallel}/T_{e\perp}$	$T_{p\parallel}/T_{p\perp}$
1	300-350	8.7 ± 4.6	14 ± 5	4.4 ± 1.8	1.1-1.2	2.0 ± 1
2	307	12.9	11.5	4.49	3.04	160
3	320	7.2	11.7	4.8	3.05	164
4	288	12	46	6.7	1.00	900
5	330		100	0.9	1.00	45
6	313		60	0.41	1.00	11
7	20	370		11		
8	290	2.7				
9	266	3.2		12		
10	258	3.34				

Model 1, the observed quiet solar wind conditions [Hundhausen *et al.*, 1970; Hundhausen, 1972a].

Model 2, from the present kinetic model (see also Lemaire and Scherer [1972c]).

Model 3, from Lemaire and Scherer's [1971b] kinetic model with an asymmetric velocity distribution.

Model 4, from Jockers's [1970] semikinetic model 3.

Model 5, from Hollweg's [1970] semikinetic model with $T_e(r) = 10^6 \text{ }^\circ\text{K}$.

Model 6, from Chen *et al.*'s [1972] semikinetic model with a spiral magnetic field and a polytropic electron temperature distribution.

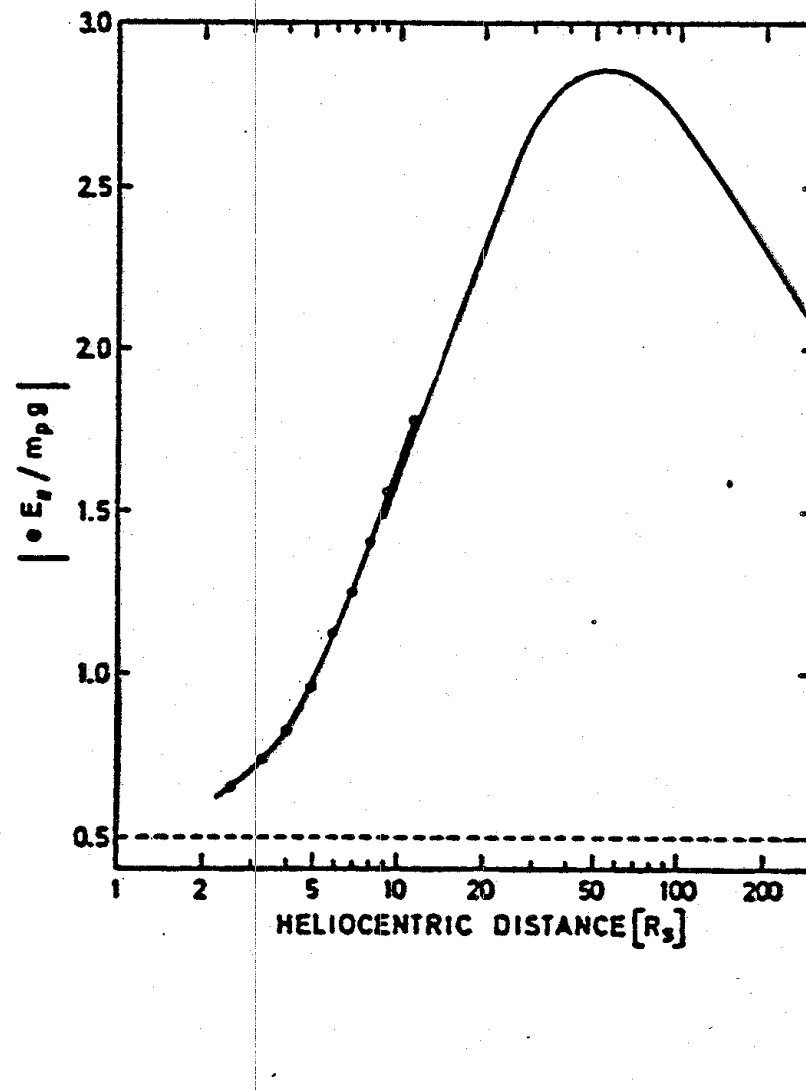
Model 7, from Chamberlain's [1960] evaporative breeze model.

Model 8, from Jensen's [1963] exospheric model.

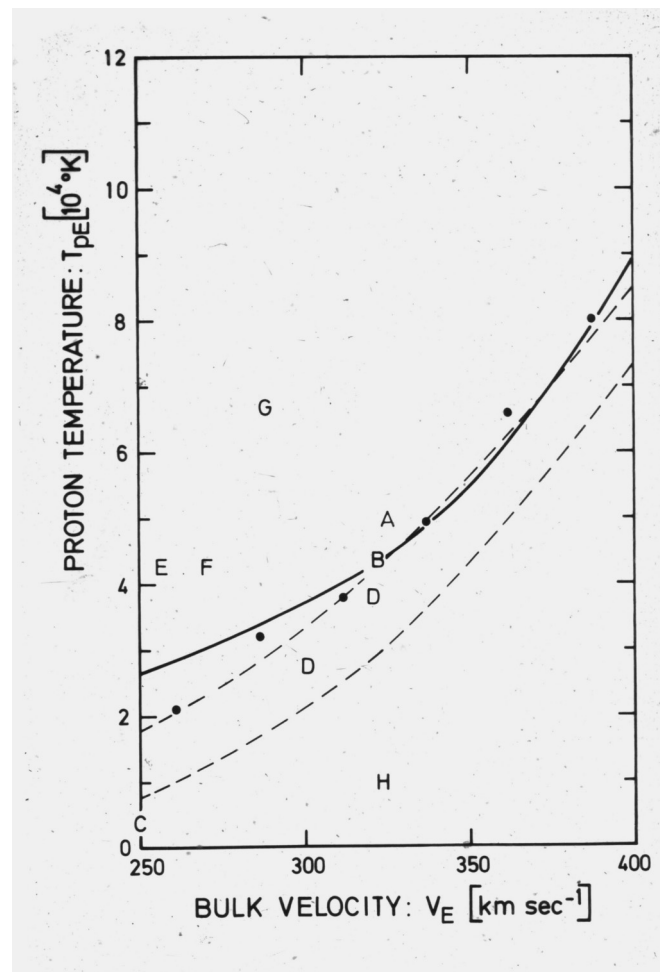
Model 9, from Brandt and Castinelli's [1966] exospheric model.

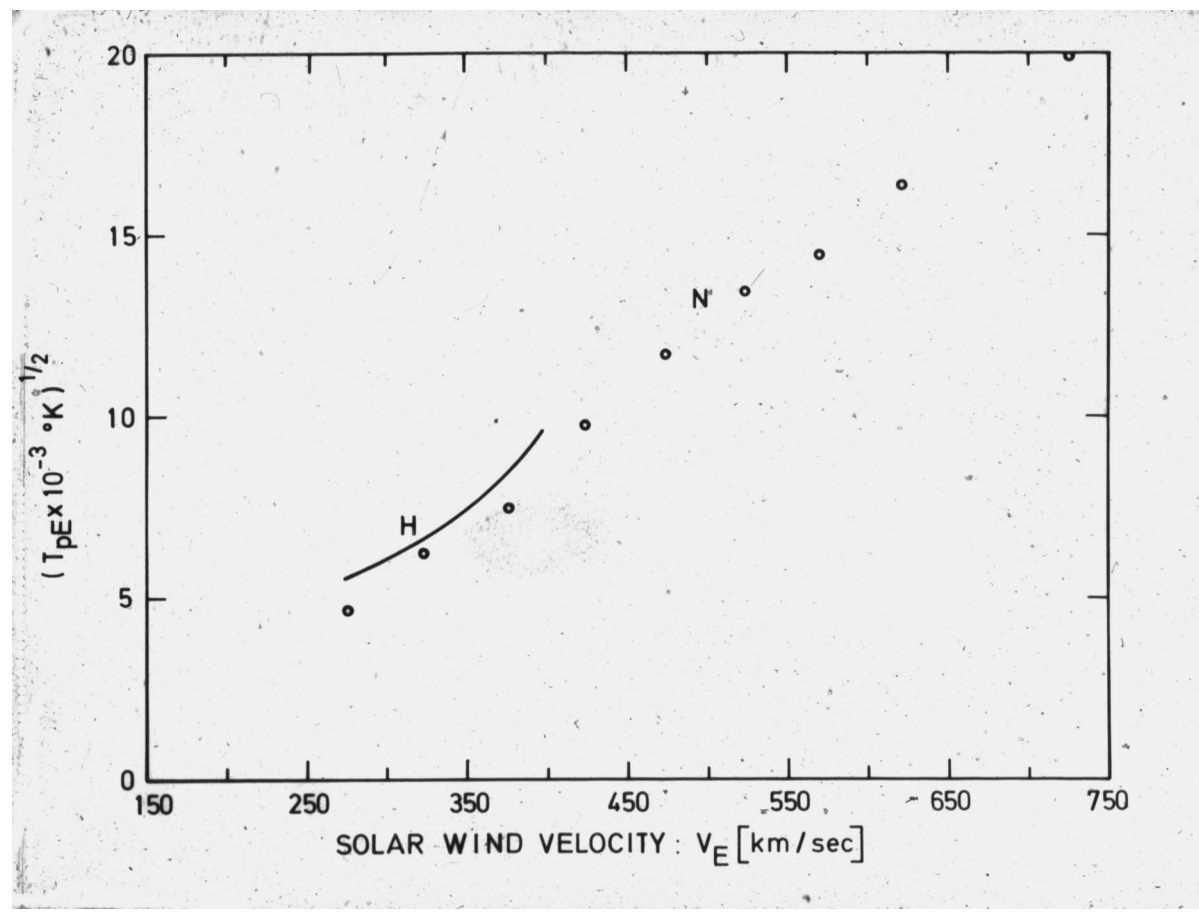
Model 10, from Sen's [1969] kinetic model.

**Ratio of Electric force over
gravitational force
acting on protons : $eE/m_p g$**

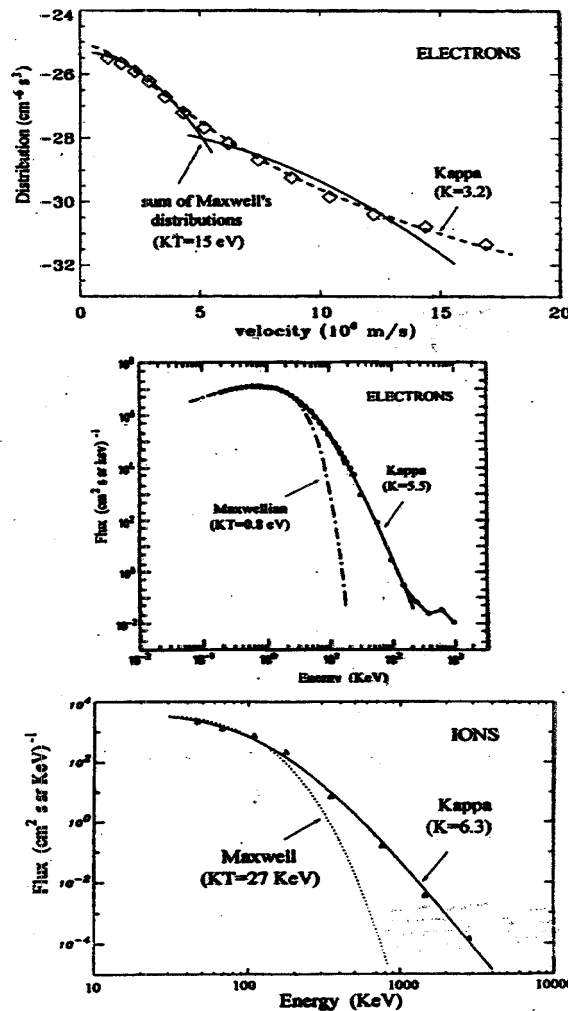


Correlation between SW proton temperature and bulk velocity at 1 AU
in slow solar wind regimes

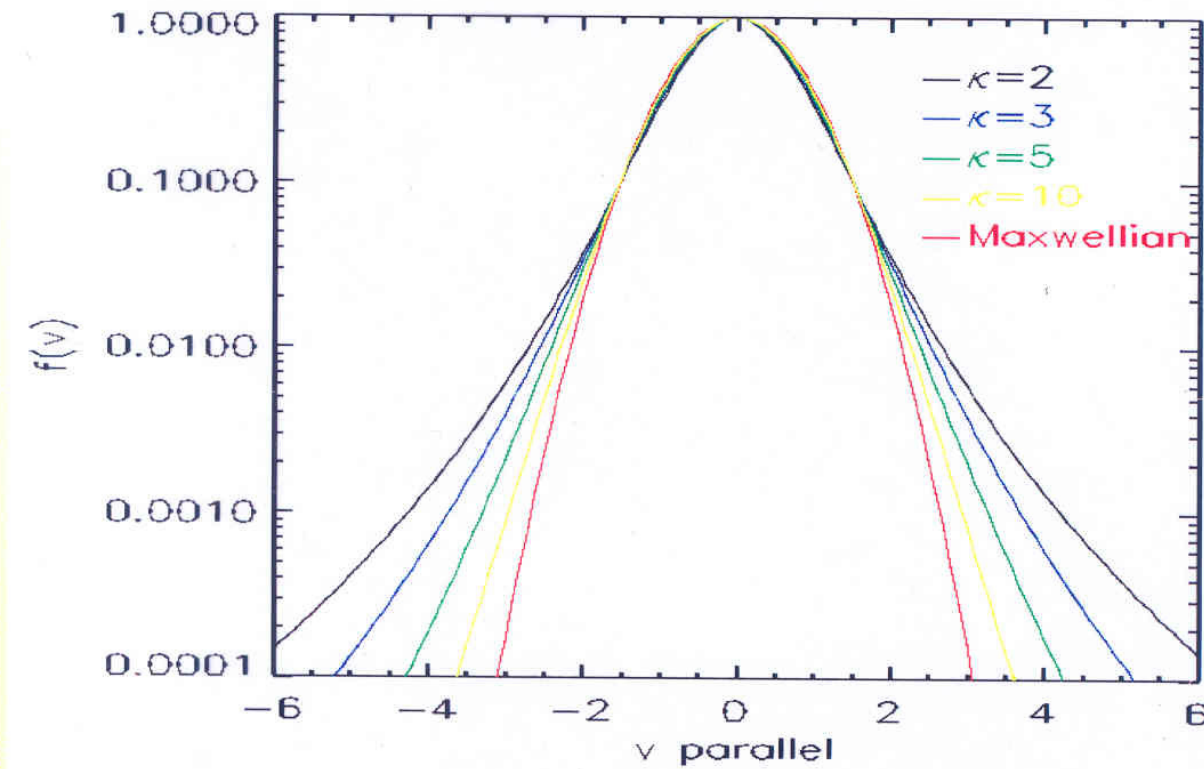




This difficulty may be partly resolved by assuming
a Lorentzian/Kappa VDF at the exobase,
instead of a Maxwellian



A small amount of additional suprathermal electrons can accelerate the solar wind to high velocities



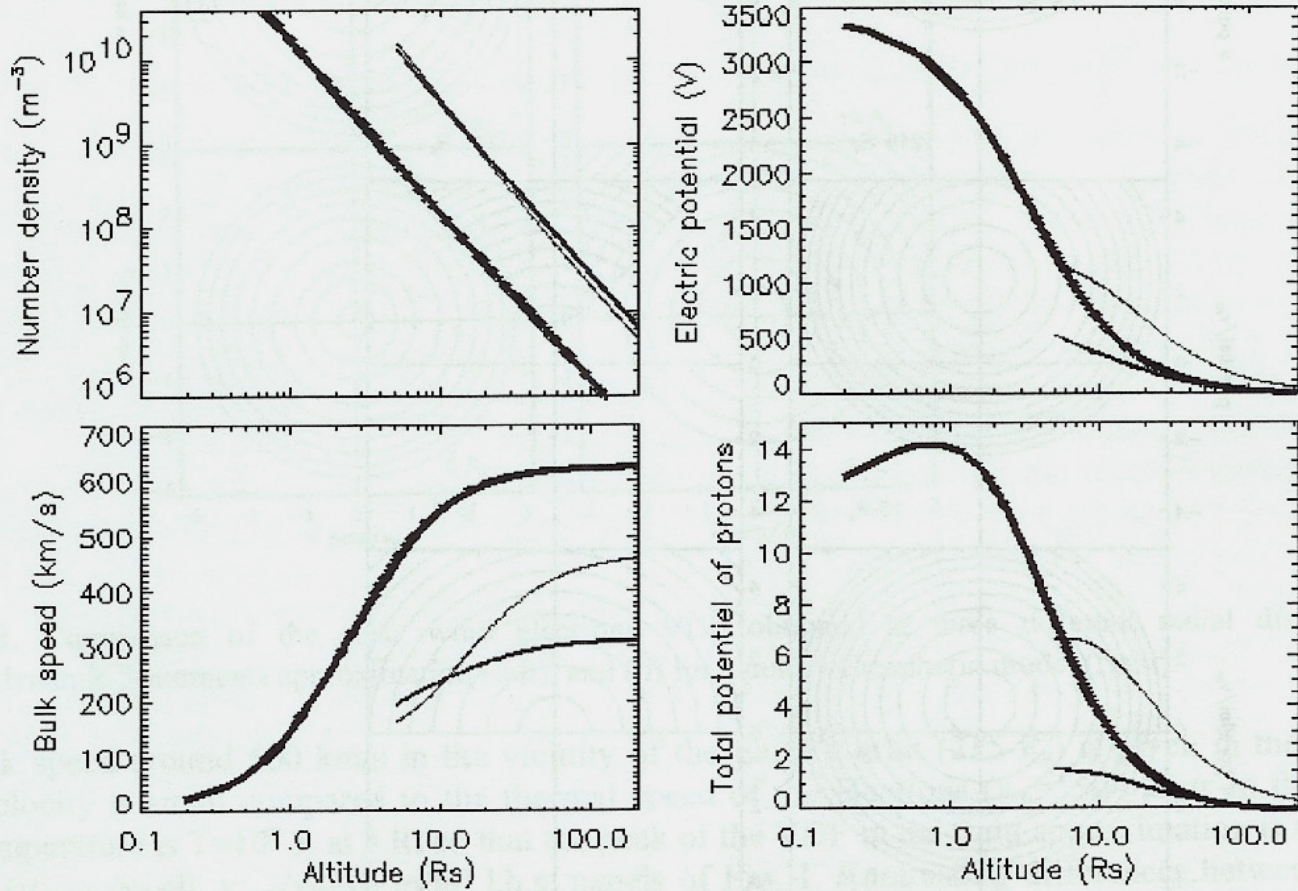


FIGURE 3. Number density (upper left panel), electrostatic potential (upper right panel), bulk speed (lower left panel) and total potential (lower right panel) of the solar wind protons as a function of the altitude above the photosphere for three different exospheric models. The first one is obtained with a Maxwellian VDF (thick lines above $5 R_s$), the second with a Lorentzian VDF with $\kappa=3$ (thin lines above $5 R_s$). The exobase altitude is located at $5 R_s$ in these two models. The bold lines starting at a heliospheric altitude of $0.1 R_s$ presents the results for a Lorentzian exospheric model with $\kappa=3$ but for an exobase altitude at $0.1 R_s$.

	r_{\max}	$V(r_{\max})$	$U(1AU)$
If $\kappa \downarrow$	↓	↑	↑
If $T_0 \uparrow$	↓	↑	↑
If $r_0 \downarrow$	↓	↑	↑

Velocity distribution functions (VDF)

Local drifting Maxwellian

(Euler or Grad 5-moment approximation)

$$f^M(\mathbf{r}, \mathbf{v}, t) = n(\mathbf{r}, t) [m / 2 \pi k T(\mathbf{r}, t)]^{3/2} \exp \{ -m [\mathbf{v} - \mathbf{u}(\mathbf{r}, t)]^2 / 2 k T(\mathbf{r}, t) \}$$

$n(\mathbf{r}, t)$: number density of particles

$\mathbf{u}(\mathbf{r}, t)$: bulk or average velocity

$T(\mathbf{r}, t)$: temperature

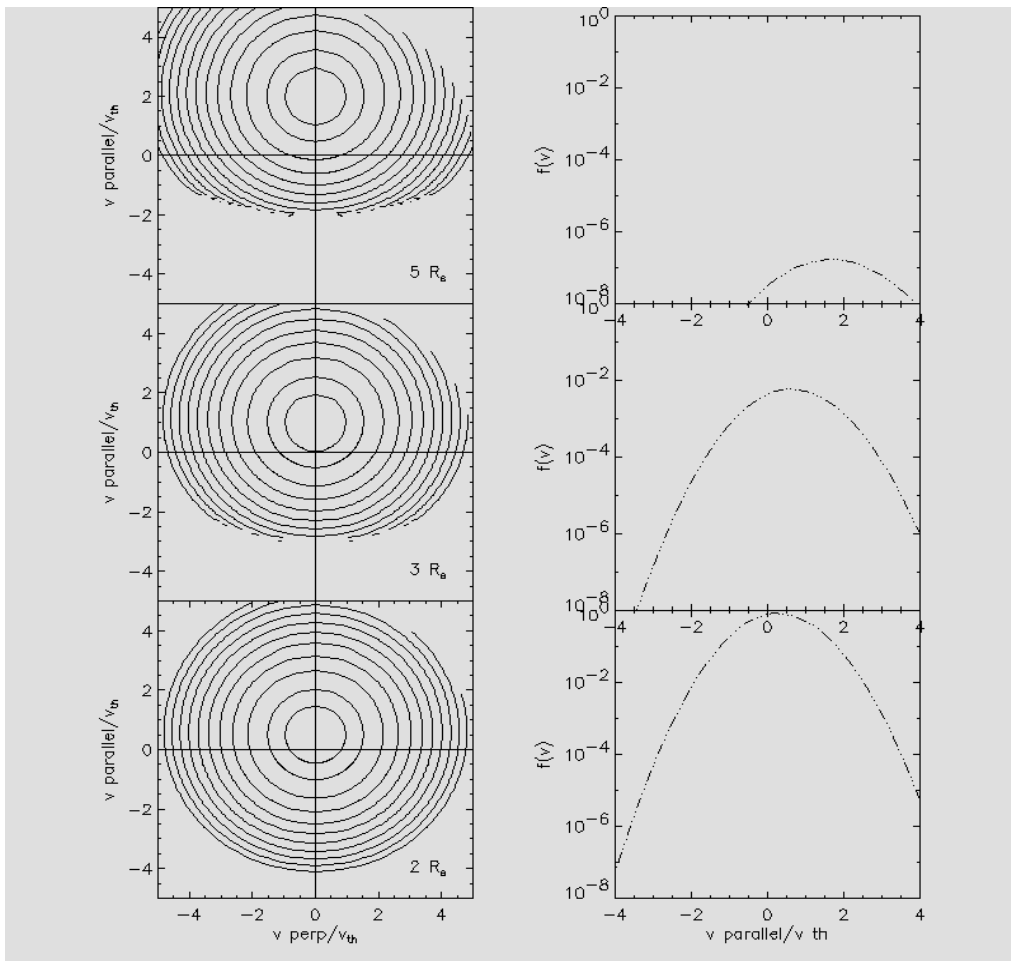
Chapman-Enskog expansion

(Normal solutions)

$$f(\mathbf{r}, \mathbf{v}, t) = f^M(\mathbf{r}, \mathbf{v}, t) [1 + \epsilon g^{(1)}(\mathbf{v}) + \epsilon^2 g^{(2)}(\mathbf{v}) ..]$$

ϵ : ordering parameter that reflects smallness of the mean free path compared to scale length of inhomogeneities in the fluid

Conductive hydrodynamic solar wind model



Noble & Scarf (1963);
Parker (1964);
Whang & Chang (1965);

...
Hydrodynamic solar wind
with wind velocity :
 $u = u(r) \neq 0$

with heat flow :
 $q = -\lambda dT/dr \neq 0$

Higher order approximations for the VDF

Grad's 20-moment approximation

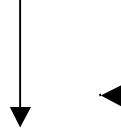
$$f = f^M(r, v, t) [1 + \beta \tau : \mathbf{c} \mathbf{c} / 2 p - \beta \mathbf{q} \cdot \mathbf{c} / p + \beta^2 \mathbf{Q} : \mathbf{c} \mathbf{c} \mathbf{c} / 6 p]$$

$$\beta = m / kT$$

p = scalar pressure

Oraevskii-Schunk 16-moments approximation

$$f = f^{BM}(r, v, t) [1 + \tau : \mathbf{c}_\parallel \mathbf{c}_\perp / 2 p - \mathbf{q}_\perp \cdot \mathbf{c}_\parallel / p + \beta_\perp^2 \mathbf{q}_\parallel \cdot \mathbf{c}_\perp / 6 p]$$



$$f^{BM}(r, v, t) = n(r, t) [\beta_\perp / 2\pi] [\beta_\parallel / 2\pi]^{1/2} \exp \{-\beta_\parallel \mathbf{c}_\parallel^2 / 2 - \beta_\perp \mathbf{c}_\perp^2 / 2\}$$

(a bi-Maxwellian VDF)

VDF observed at 1 AU by Helios and modeled
by a 16-moment approximation (Demars & Schunk, 1990)

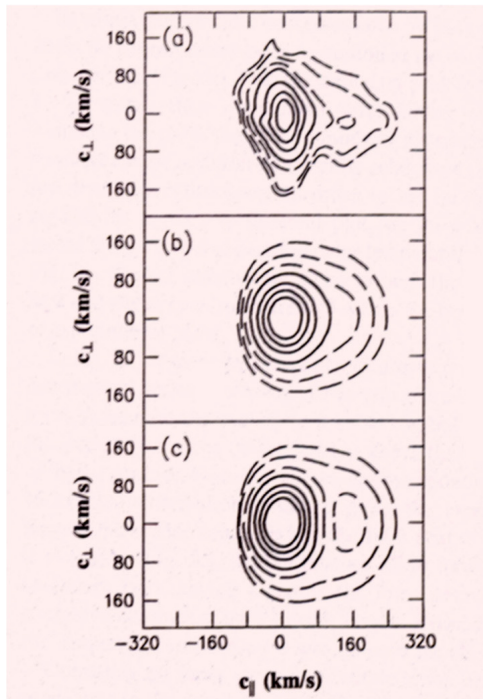


FIG. 5. EXPERIMENTAL AND 16-MOMENT CONTOUR PLOTS FOR THE CASE IN WHICH A SECONDARY PEAK EXISTS AT THE LEVEL OF CONTOUR 0.1.

The experimental plot (a), adapted from case C2 of Marsch *et al.* (1982), corresponds to the following parameter values: $u = 675 \text{ km s}^{-1}$, $n = 6.7 \text{ cm}^{-3}$, $T_{pi} = 399,000 \text{ K}$, $T_{p\perp} = 319,000 \text{ K}$, and $q_p = 0.149 \times 10^{-2} \text{ erg cm}^{-2} \text{ s}^{-1}$. The 16-moment plot (b) is generated using these experimental values with the further assumption that $q_p^{\parallel}/q_p^{\perp} = 10$. The 16-moment plot (c) uses the same values as (b) except that $q_p = 0.23 \times 10^{-2} \text{ erg cm}^{-2} \text{ s}^{-1}$.

Kinetic SW models

Exospheric models

Maxwellian VDF

Lorentzian VDF

Fokker-Planck models

...used to determine/model VDF in transition region
i.e. where Kn increases from $Kn \ll 1 \Rightarrow Kn \gg 1$

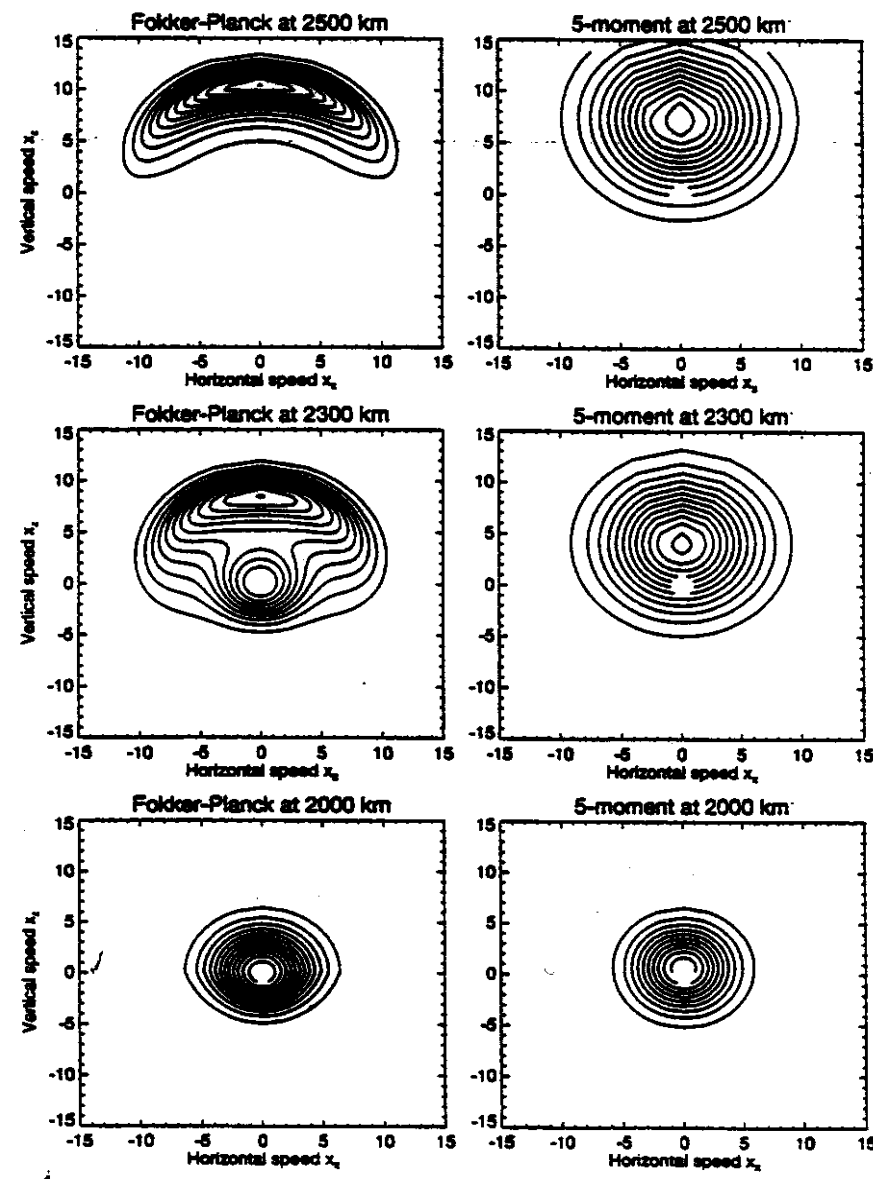
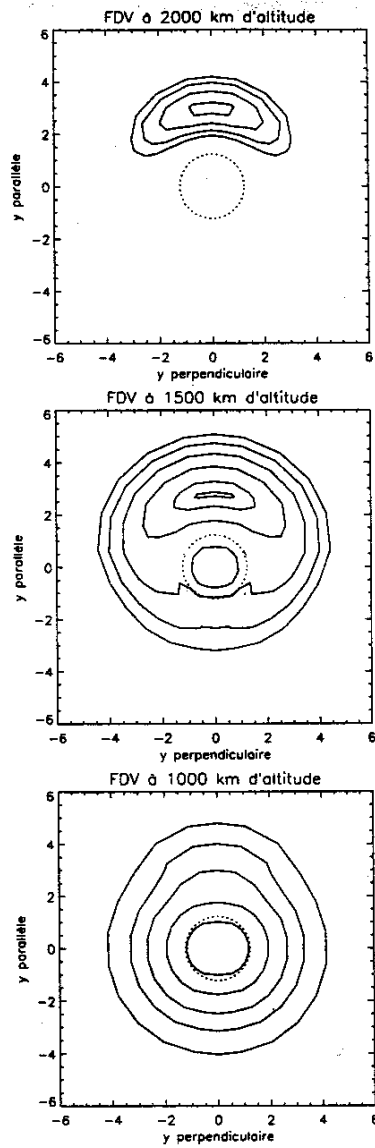
Fokker–Planck equations for protons in polar wind

Finite difference solution of VDF
(Lie-Svensden & Rees, 1998)

Legendre polynomial + Speed polynomial expansion of VDF
(Pierrard & Lemaire, 1998)

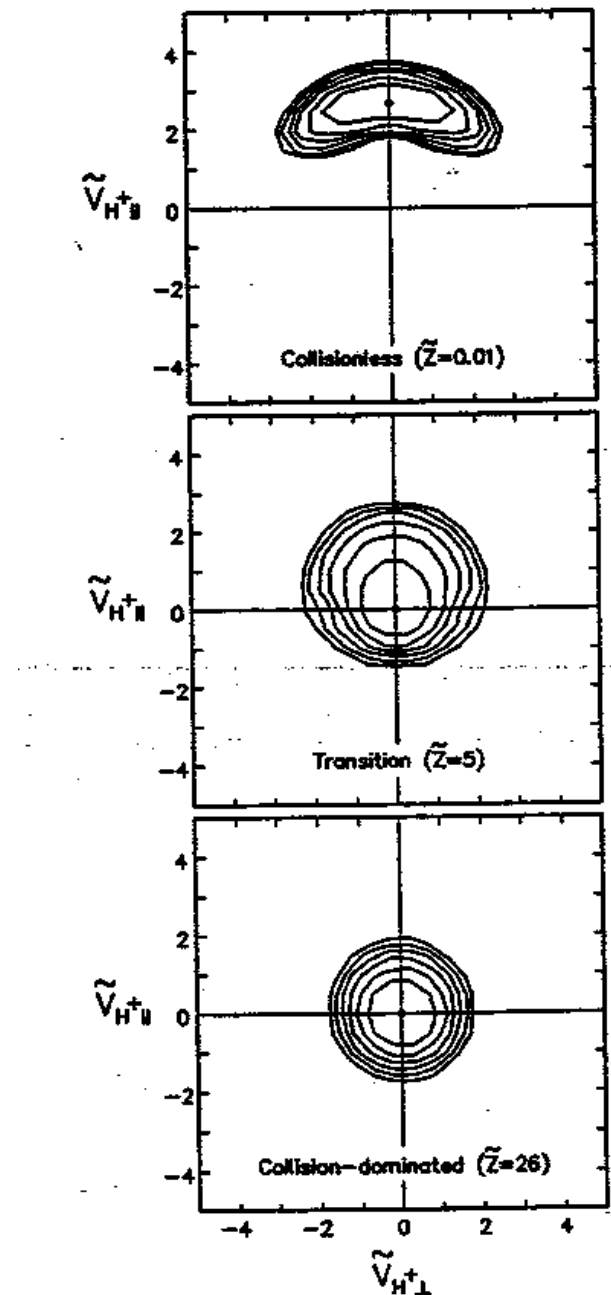
$$f(r, y, \mu) = f^M \left[\sum_{l=0}^{n-1} \sum_{s=0}^{N-1} a_{ls}(r) P_l(\mu) S_s(y) \right]$$

$$\begin{aligned} y^2 &= m v^2 / 2 k T \\ \mu &= \cos \theta \end{aligned}$$



Pierrard & Lemaire, 1998

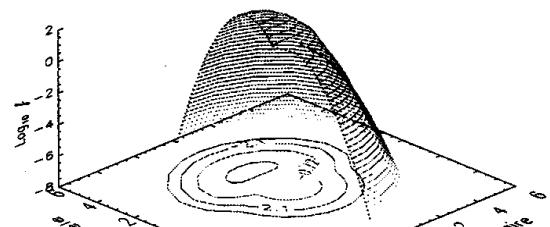
Lie-Svendsen & Leer, 1998



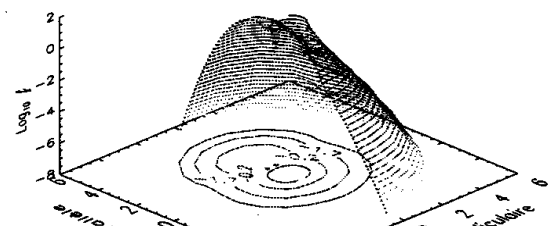
Monte Carlo simulation
protons diffusing across
background of O⁺ ions in
polar wind
(Barakat *et al*, 1996)

Solution of Fokker-Planck equation for protons in polar wind

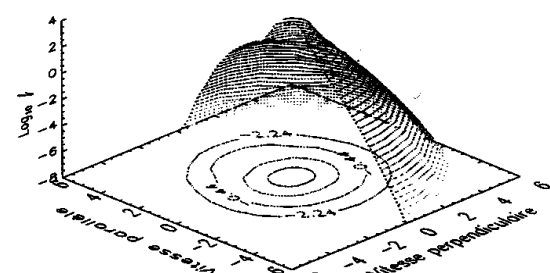
Fonction de distribution des vitesses à 2000 km



Fonction de distribution des vitesses à 1750 km



Fonction de distribution des vitesses à 1500 km



- VDF at low altitude : only one main Maxwellian peak at $v = 0$ (like in the case of hydrostatic equilibrium)
- Upward flux of particles and energy is carried by the higher velocities: escaping particles; Note the asymmetry of particles with higher velocities in the vertical direction...
- A secondary peak develops at intermediate altitudes; it becomes prominent at high altitude; while the low velocity peak vanishes gradually and disappears in the exosphere...

Summary (1)

Exospheric models are zero-order kinetic models; they are useful

- to understand basic kinetic aspects
- to model properly the evolution of the VDF when Kn is not small
- to evaluate the escape of ions out of corona and topside ionosphere,
- to demonstrate the existence of a polarization electrostatic potential induced by the gravitational force (or other mechanisms...)
- to show how this electrostatic force accelerates the ions polar and solar wind ions to supersonic velocities

Summary (2)

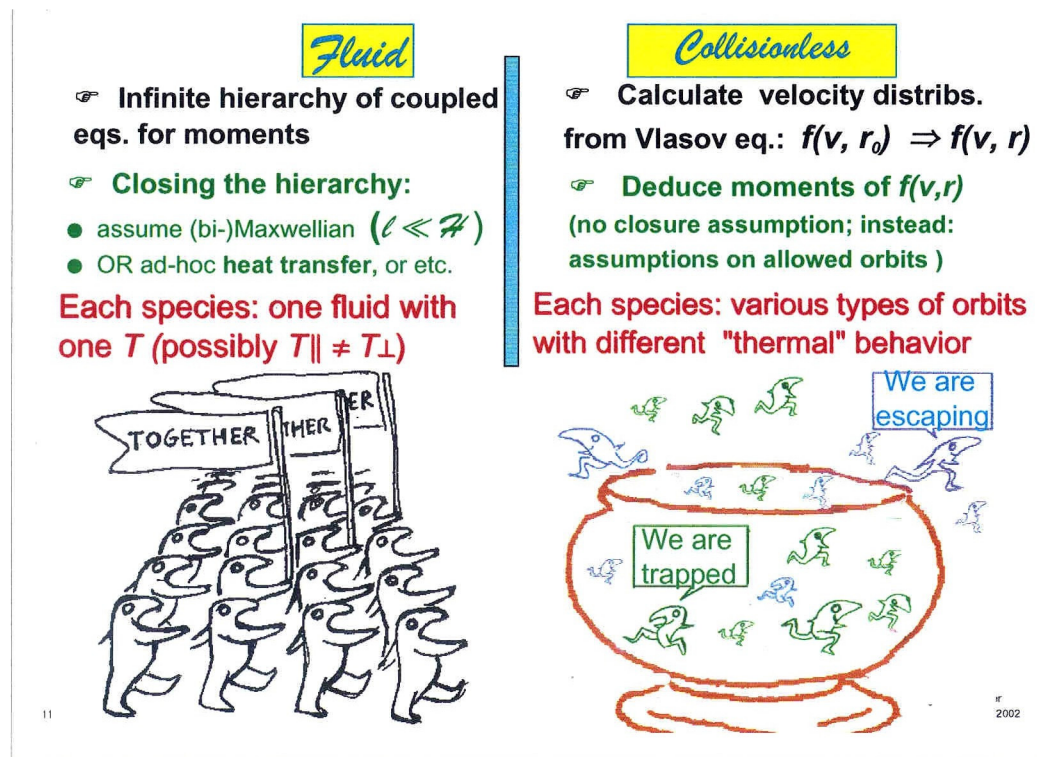
- First order kinetic theories (Fokker-Planck, and Monte Carlo simulations, ...) demonstrate that across the exobase transition region the shape of the VDF changes from a nearly Maxwellian with a single peak at $v = 0$, into a doubly peaked VDF; this emerging second peak is contributed by escaping suprathermal protons; the emerging bean shaped peak becomes more and more prominent; eventually at higher altitudes it overtakes the primary peak of low energy ballistic particle population trapped by the potential barrier.
- This previously unsuspected transformation of the VDF across the transition region is very different from a drifting Maxwellian whose peak velocity $u(r)$ gradually increases with the altitude, as assumed in hydrodynamic models which are based on the Chapman-Enkog's and Grad's expansions of the VDF.

Summary (3)

- Kinetic models (Exospheric, Monte Carlo, Fokker-Planck solutions, ...) are more detailed microscopic descriptions of the VDFs. They are complementary to fluid/moment approaches
- Kinetic models can be fitted to hydrodynamical solutions which are fully satisfactory at lower altitudes, i.e. below the exobase.
- Finite difference solutions as well as polynomial expansions of the Fokker-Planck equations are physically more appropriate for the physicist who wants to understand the change of the VDF in transition regions;
- Time dependent kinetic models have not yet been worked out, while they are currently developed for hydrodynamic models of the SW and PW.

Hydrodynamic/fluid streaming *versus* Kinetics evaporation

a cartoon by F. Meyer-Vernet



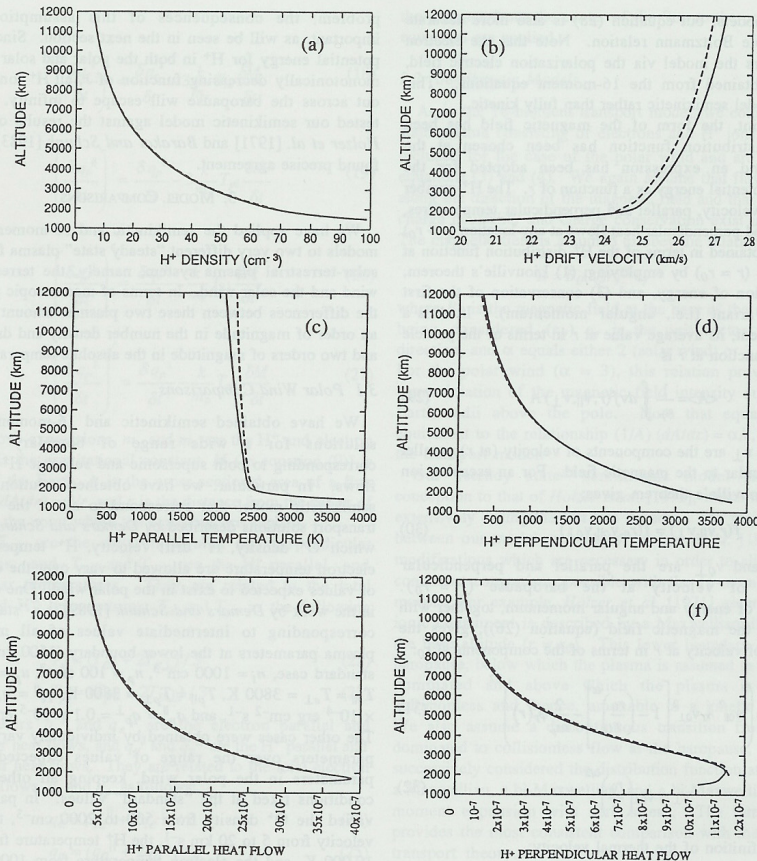
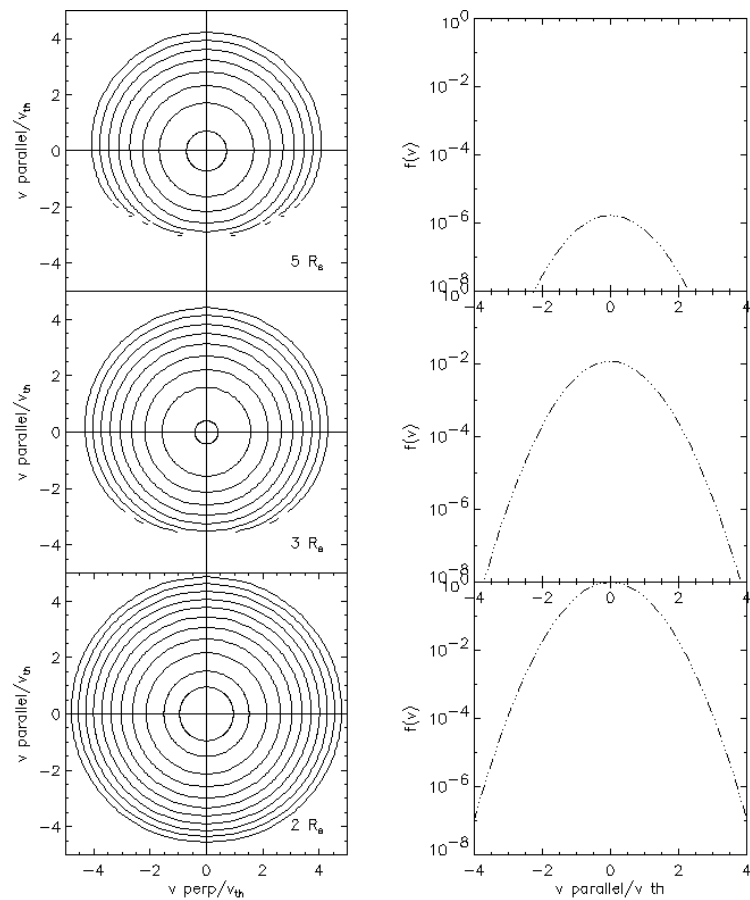


Fig. 1. H⁺ parameter profiles obtained from the semikinetic (dashed curves) and the 16-moment transport (solid curves) models for the supersonic polar wind outflow. Boundary conditions for both models at an altitude of 1500 km (the baropause) are $n(O^+)=1000 \text{ cm}^{-3}$, $n_p=100 \text{ cm}^{-3}$, $u_p=20 \text{ km s}^{-1}$, $T_{p\parallel}=T_{p\perp}=3800 \text{ K}$, and $q_p^\parallel=q_p^\perp=0.1 \times 10^{-5} \text{ erg cm}^{-2} \text{ s}^{-1}$, where the subscript p refers to the H⁺ ions. In addition, the 16-moment transport model assumes that $T_{e\parallel}=T_{e\perp}=3800 \text{ K}$ and $q_e^\parallel=q_e^\perp=-0.11 \times 10^{-4} \text{ erg cm}^{-2} \text{ s}^{-1}$, where the subscript e refers to the electrons. Shown are (a) number density, (b) drift velocity, (c) parallel temperature, (d) perpendicular temperature, (e) parallel heat flow, and (f) perpendicular heat flow. The semikinetic model assumes a 16-moment distribution function with zero stress at 1500 km. (Adapted from Demars and Schunk [1991b].)

VDF of coronal protons
 in Chapman's conductive hydrostatic equilibrium
 at 3 radial distances



$$\xi = 0$$

$$T(r) = T_0 \{ r_o / r \}^{2/7}$$

Chapman hydrostatic model :

No wind velocity : $\mathbf{u} = 0$

Conductive heat flow :

$$q = -\lambda \frac{dT}{dr}$$

VDF observed at 1 AU by Helios and modeled
by a 16-moment approximation (Demars & Schunk, 1990)

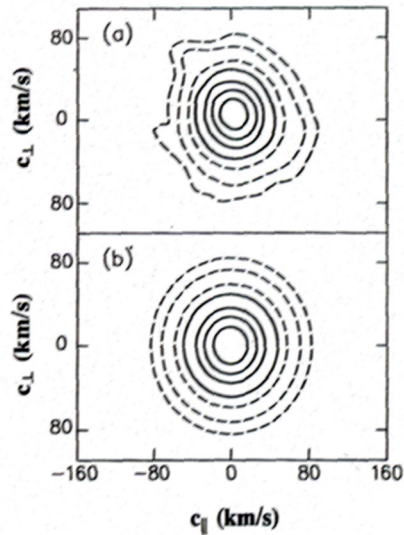
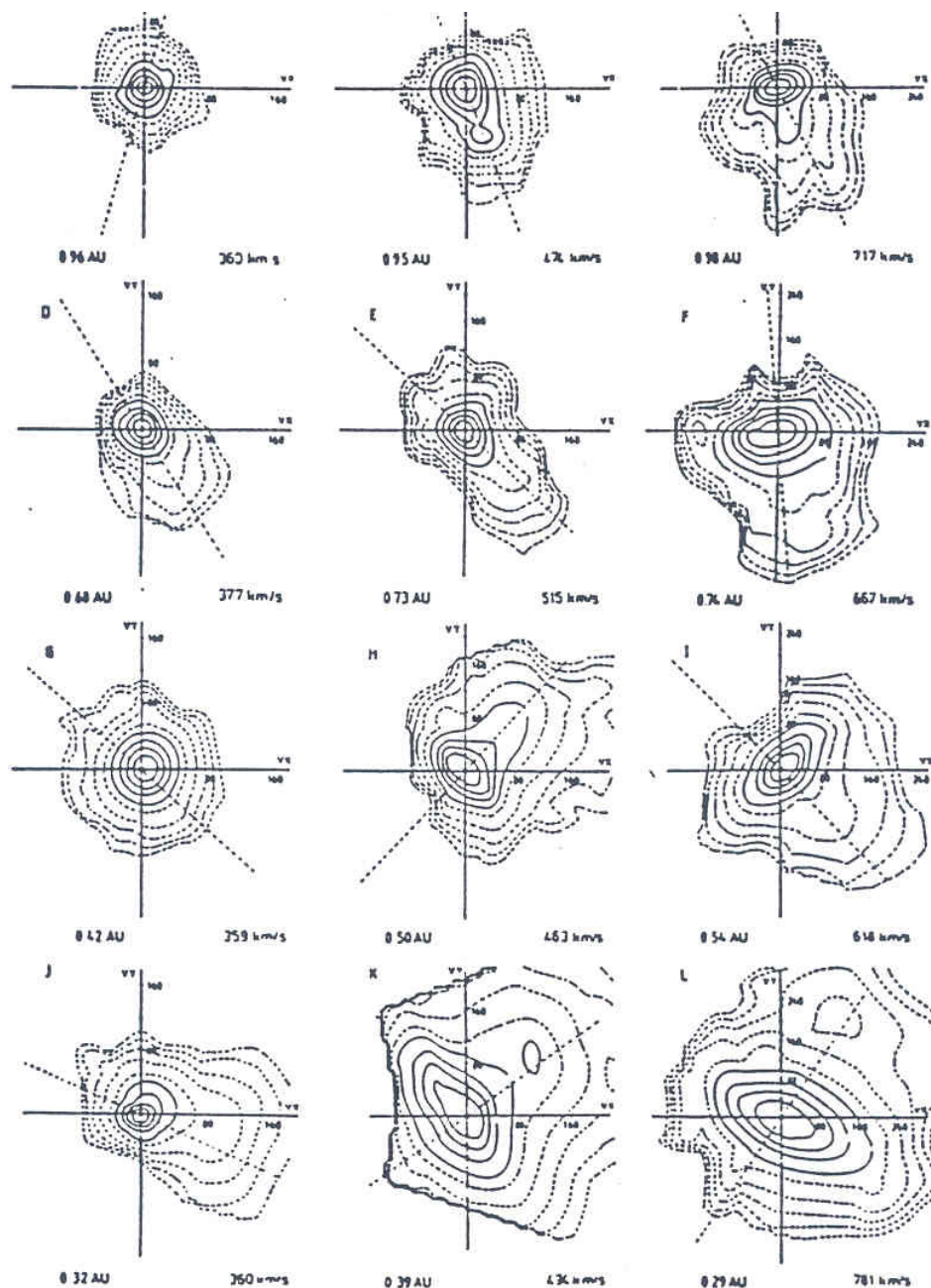


FIG. 1. EXPERIMENTAL AND 16-MOMENT CONTOUR PLOTS FOR THE CASE OF AN ISOTROPIC DISTRIBUTION.

The experimental plot (a), adapted from case G of Marsch *et al.* (1982), corresponds to the following parameter values: $u = 359 \text{ km s}^{-1}$, $n = 139.6 \text{ cm}^{-3}$, $T_{p\parallel} = 75,000 \text{ K}$, $T_{p\perp} = 80,000 \text{ K}$, and $q_p = 0.208 \times 10^{-3} \text{ erg cm}^{-2} \text{ s}^{-1}$. The 16-moment plot (b) is generated using these experimental values with the further assumption that $q_p^\parallel/q_p^\perp = 1$. In this and subsequent figures, the contour levels are 0.8, 0.6, 0.4, and 0.2 (solid curves), and 0.1, 0.032, and 0.01 (dashed curves). The contour levels decrease systematically from the maximum.



- there are many different ways to approximate VDF of electrons and ions in space plasmas
- Euler approximation or 5-moment approximation is OK if one needs to calculate only the distributions of lower order moments of VDF (densities and bulk velocities)
- Higher order expansions of VDF are required to model correctly the asymmetry and skewness of VDF in collisionless plasmas
- The moments determined in kinetic approach (exospheric, FP, Monte Carlo ...) satisfy the full (untruncated) hierarchy/set of moments equations

tain steady state solutions for the H^+ ion velocity distribution function.

First, we expand the solution in Legendre polynomials with respect to μ or $\cos\theta$ [Canuto *et al.*, 1988]:

$$f(r, y, \mu) = \sum_{l=0}^{n-1} f_l(r, y) P_l(\mu). \quad (21)$$

Calculating

$$\int_{-1}^1 \left[\mathcal{D}f = \left(\frac{df}{dt} \right)_c \right] P_{l'}(\mu) d\mu \quad (22)$$

and taking into account the orthogonality properties of the Legendre polynomials:

$$\int_{-1}^1 P_l(\mu) P_{l'}(\mu) d\mu = \frac{2}{2l+1} \delta_{ll'}, \quad (23)$$

the equation is decomposed into n partial differential equations where the n unknowns are $f_l(r, y)$:

$$\begin{aligned} & w_{H^+} y \left(\beta_1(l) \frac{\partial f_{l-1}}{\partial r} + \beta_2(l) \frac{\partial f_{l+1}}{\partial r} \right) \\ & + \frac{a(r)}{w_{H^+}} \left(\beta_1(l) \frac{\partial f_{l-1}}{\partial y} + \beta_2(l) \frac{\partial f_{l+1}}{\partial y} \right) \\ & + \left(\frac{a(r)}{yw_{H^+}} + \frac{3}{2} \frac{w_{H^+} y}{r} \right) \left(\beta_3(l) f_{l-1} + \beta_4(l) f_{l+1} \right) \\ & = C_0 \left[\frac{1}{y^2} \frac{\partial}{\partial y} \left\{ \left(2y f_l \frac{T_{H^+}}{T_{O^+}} + \frac{\partial f_l}{\partial y} \right) \mathcal{F} \left(\frac{w_{H^+}}{w_{O^+}} y \right) \right\} \frac{2}{2l+1} \right. \\ & \quad \left. + \frac{1}{y^3} \frac{\partial g}{\partial y} \left(\frac{-2l(l+1)}{2l+1} f_l \right) \right] \end{aligned} \quad (24)$$

Using these variables the Fokker-Planck, (1) becomes

$$\begin{aligned} & \frac{\partial f}{\partial t} + w_{H^+} y \mu \frac{\partial f}{\partial r} + \frac{a(r)}{w_{H^+}} \left(\mu \frac{\partial f}{\partial y} + \frac{(1-\mu^2)}{y} \frac{\partial f}{\partial \mu} \right) \quad \text{with } C_0 = \frac{n_{O^+} c_0}{m_{H^+}^2} \exp(-q_{O^+}(r)) \left(\frac{m_{O^+}}{2kT_{O^+}} \right)^{3/2} \left(\frac{w_{O^+}}{w_{H^+}} \right)^4 \\ & + \frac{3}{2} w_{H^+} \frac{y}{r} (1-\mu^2) \frac{\partial f}{\partial \mu} \\ & = \frac{c_0}{m_{H^+}^2} n_{O^+} \exp(-q_{O^+}(r)) \left(\frac{m_{O^+}}{2kT_{O^+}} \right)^{3/2} \left(\frac{w_{O^+}}{w_{H^+}} \right)^4 \\ & \times \left[\frac{1}{y^2} \frac{\partial}{\partial y} \left\{ \left(2y f \frac{T_{H^+}}{T_{O^+}} + \frac{\partial f}{\partial y} \right) \mathcal{F} \left(\frac{w_{H^+}}{w_{O^+}} y \right) \right\} \right. \\ & \quad \left. + \frac{1}{y^3} \frac{\partial g}{\partial y} \frac{\partial}{\partial \mu} (1-\mu^2) \frac{\partial f}{\partial \mu} \right]. \end{aligned} \quad (20)$$

$$\beta_1(l) = \frac{2l}{(2l+1)(2l-1)} \quad (25)$$

$$\beta_2(l) = \frac{2(l+1)}{(2l+1)(2l+3)} \quad (26)$$

$$\beta_3(l) = \frac{-2(l-1)l}{(2l+1)(2l-1)} \quad (27)$$

$$\beta_4(l) = \frac{2(l+1)(l+2)}{(2l+1)(2l+3)}. \quad (28)$$

This equation is similar to that derived in the article of Shizgal *et al.* [1986]. It can also be reduced to the Fokker-Planck equation used in Lie-Svendsen and Rees [1996].

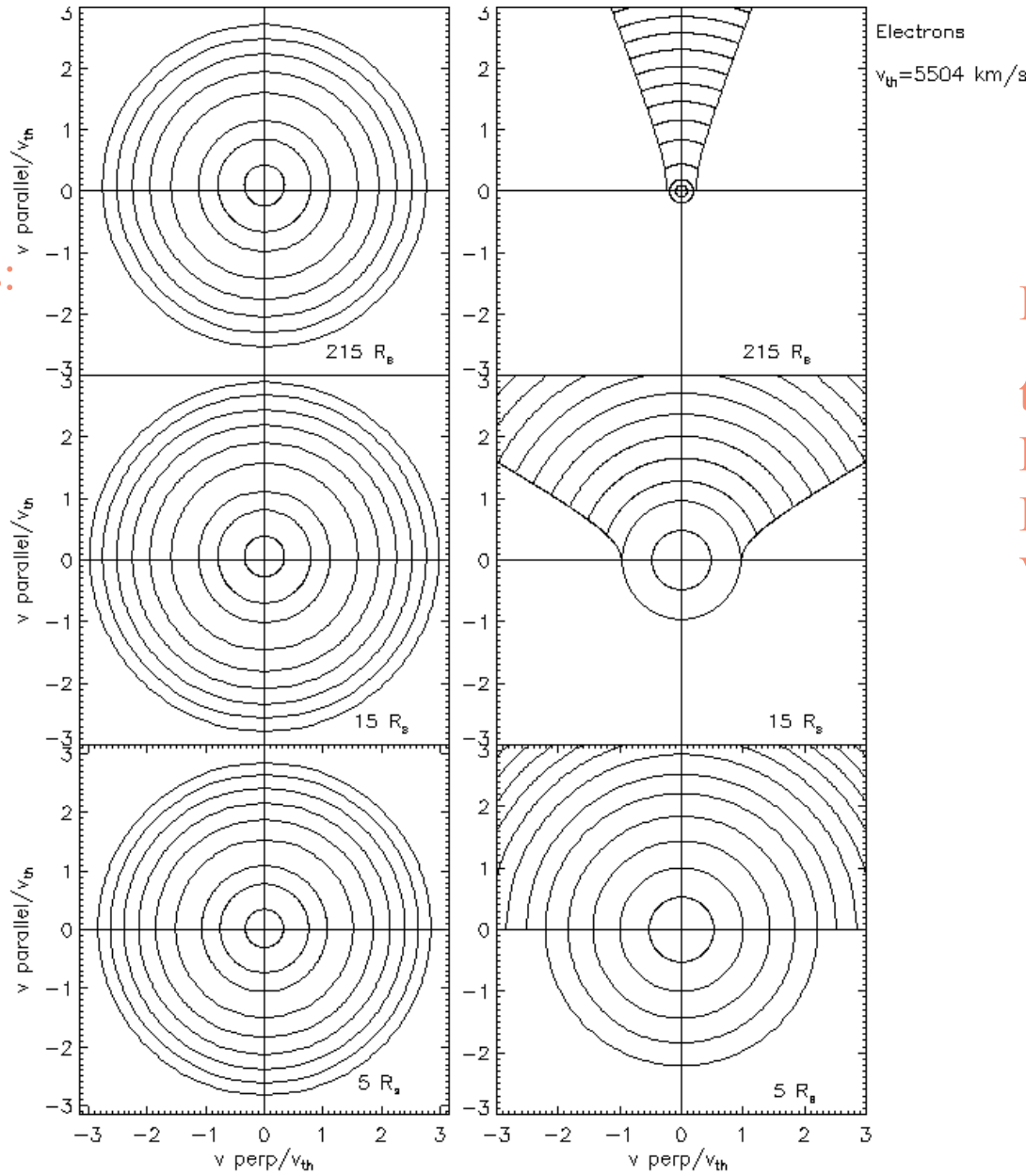
3. Method of Resolution

We have used a specialized spectral method to solve the partial differential equation (20) in (r, y, μ) and ob-

tain steady state solutions for the H^+ ion velocity distribution function. To determine the dependence of f_l on y , we introduce another spectral decomposition. The partial derivatives with respect to the y variable are expanded using the quadrature differential method (QDM) or discrete ordinate (DO) method outlined by Shizgal [1981], Shizgal and Blackmore [1984], Mansell *et al.* [1993], and Shizgal and Chen [1996; 1997].

Grad 5-moments:

displaced
Maxwellian
Electron
VDF

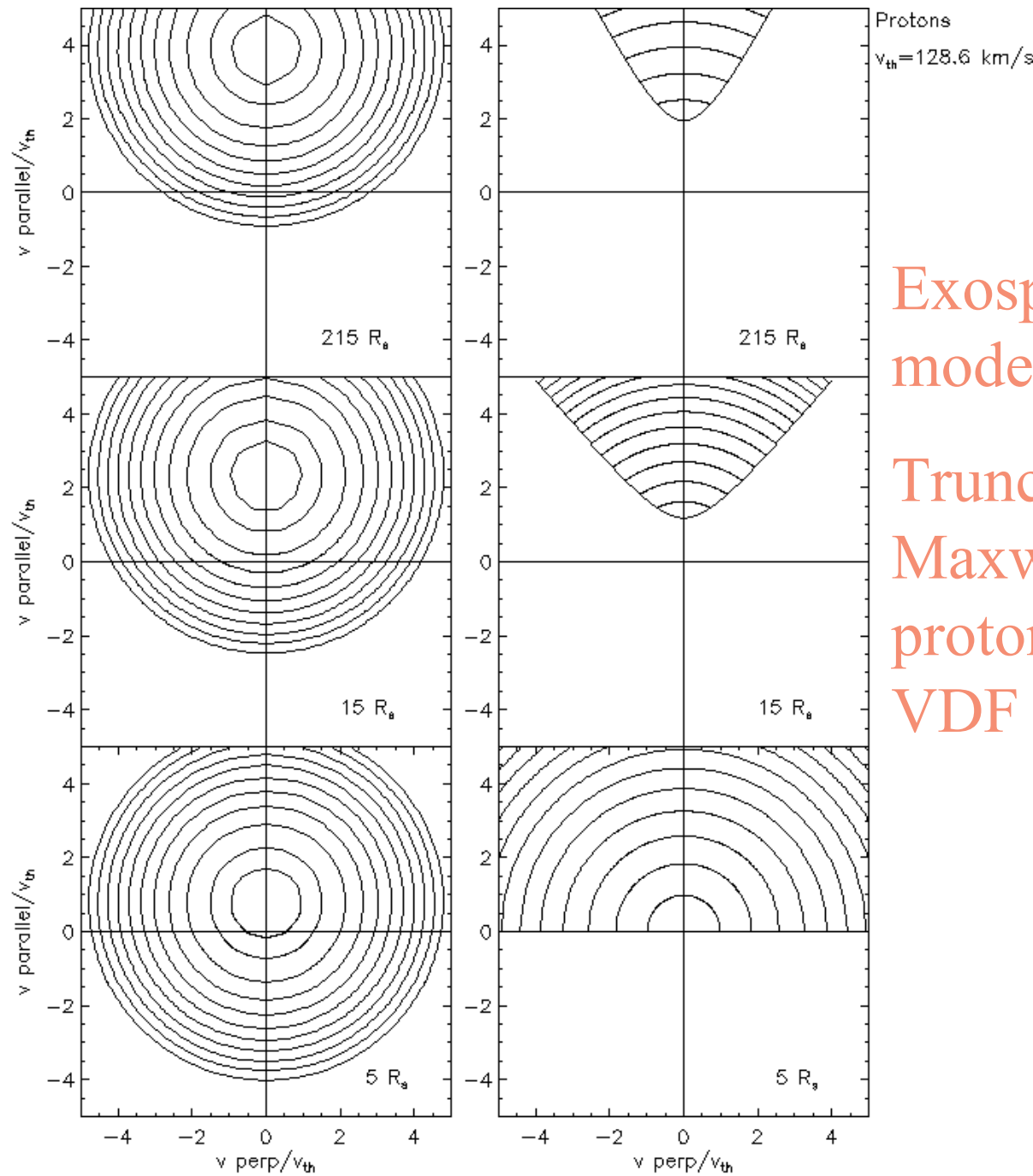


Exospheric model:
truncated
Maxwellian
Electron
VDF

It is difficult to integrate the 20-moment transport equations from the collision dominated region to the collisionless one due to the additional saddle, nodal and focal points of singularity inherent in these equations

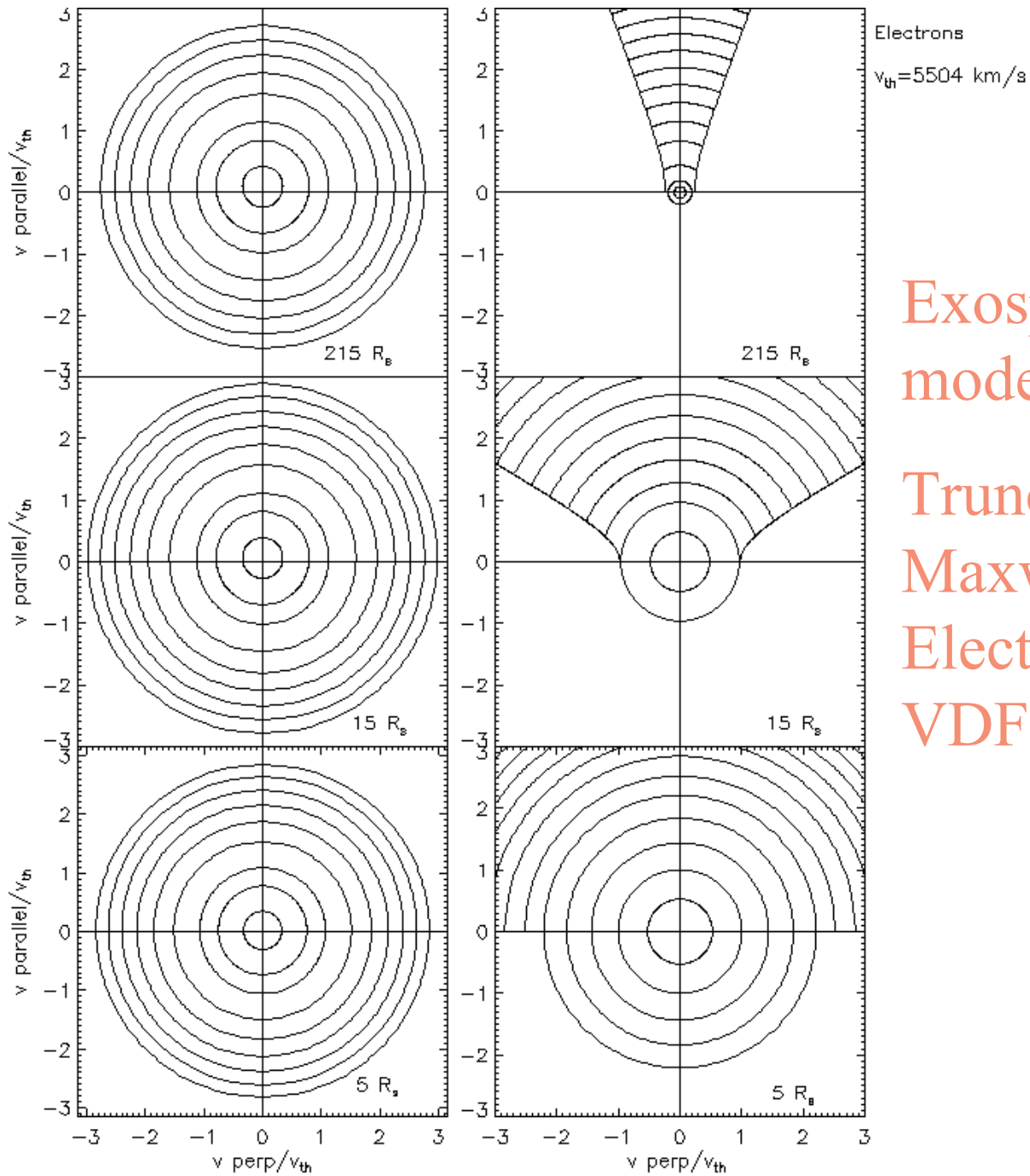
The solutions of hydrodynamic, generalized moment equations and kinetic equations depend drastically on the boundary conditions adopted at the base of the integration domain, as well as at large radial distances

5-moments Displaced Maxwellian proton VDF

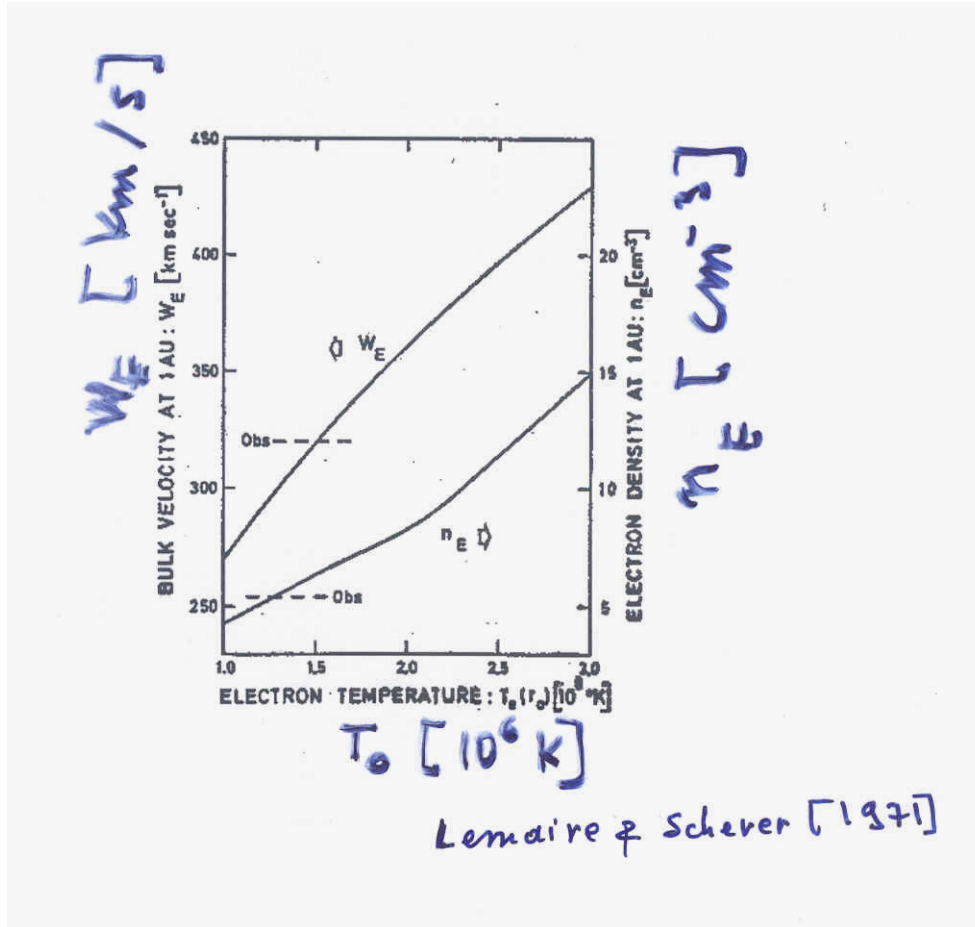


Exospheric
model:
Truncated
Maxwellian
proton
VDF

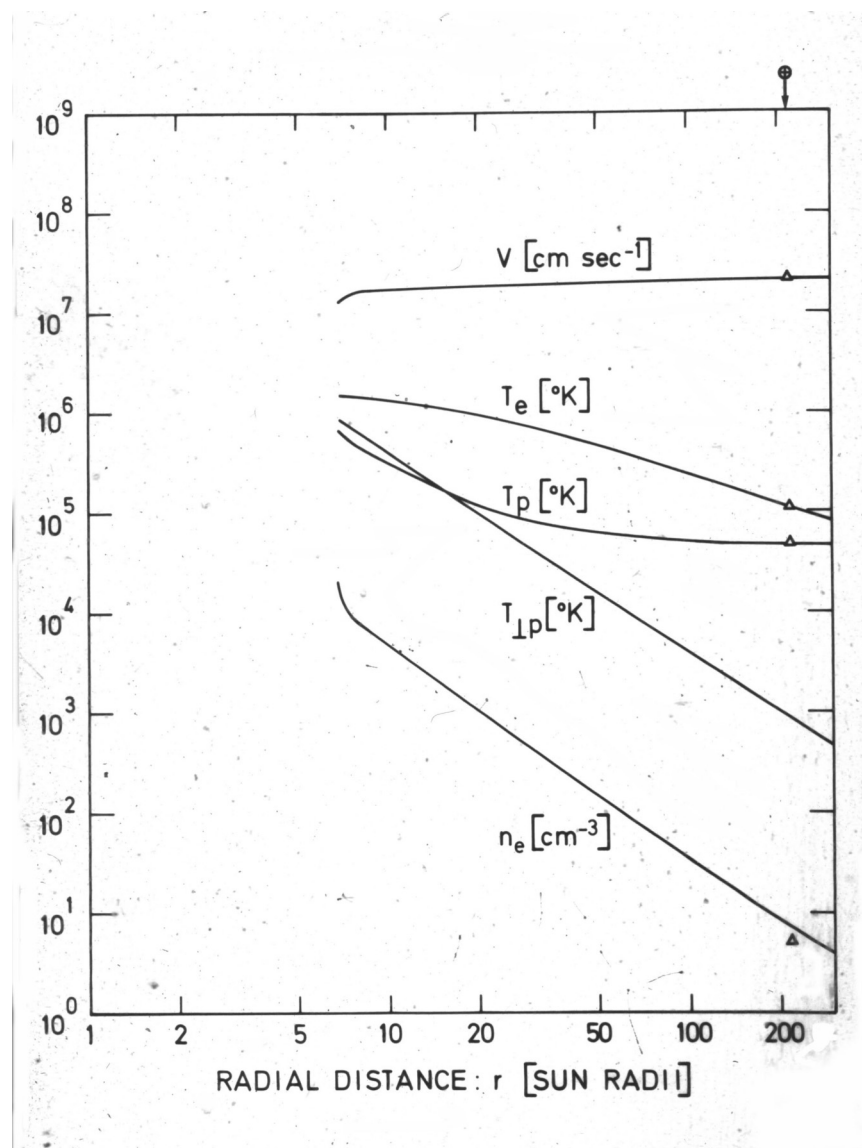
5-moments: Displaced Maxwellian Electron VDF



Exospheric model: Truncated Maxwellian Electron VDF



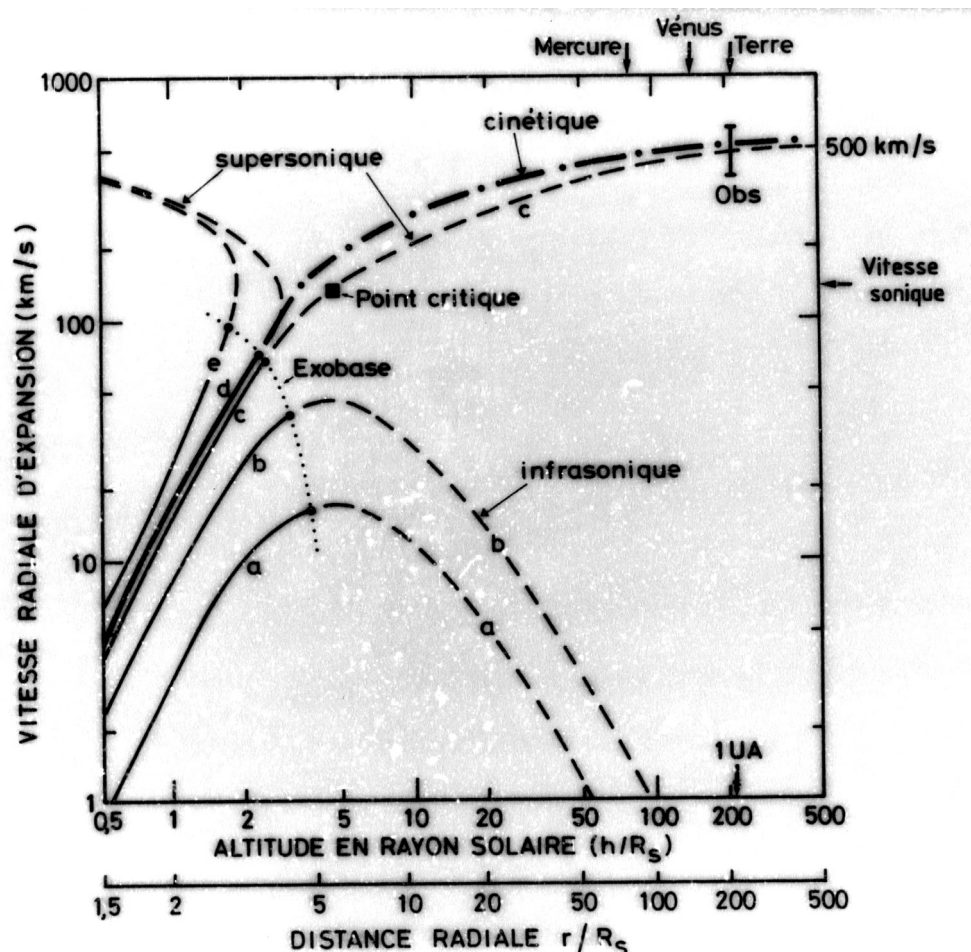
Exospheric radial distributions



Beyond the exobase Coulomb collisions become rare and can be neglected in zero order approximation and zero order kinetic models.

Hydrodynamic/fluid approximations of the transport of mass, momentum and energy are questionable in the collisionless exosphere;

Kinetic approaches are then recommended in the exosphere
 (exospheric, Fokker-Planck solutions, Monte-Carlo ...)



Advantages

- Exospheric approach explains the physical origin of the E-field that accelerates the ions in solar wind
- Predicts the correct density, bulk speed, mean temperatures; energy flux of e^- & p^+ at 1AU
- Predicts observed correlation between bulk speed and proton temperatures observed at 1 AU

$$\begin{aligned}
\frac{3}{2} kT_s &= \frac{1}{2} m_s \langle c_s^2 \rangle, && \text{species temperature;} \\
\mathbf{q}_s &= \frac{1}{2} n_s m_s \langle \mathbf{c}_s^2 \mathbf{c}_s \rangle, && \text{heat flow vector;} \\
\mathbf{P}_s &= n_s m_s \langle \mathbf{c}_s \mathbf{c}_s \rangle, && \text{pressure tensor;} \\
\boldsymbol{\tau}_s &= \mathbf{P}_s - p_s \mathbf{I} && \text{stress tensor;} \\
\boldsymbol{\mu}_s &= \frac{1}{2} n_s m_s \langle \mathbf{c}_s^2 \mathbf{c}_s \mathbf{c}_s \rangle, && \text{higher-order pressure tensor;} \\
\mathbf{Q}_s &= n_s m_s \langle \mathbf{c}_s \mathbf{c}_s \mathbf{c}_s \rangle, && \text{heat flow tensor;}
\end{aligned}$$

where n_s is the density of species s , $p_s = n_s k T_s$ is the partial pressure, k is Boltzmann's constant, \mathbf{I} is the unit dyadic, and the bracket symbol denotes the average

$$\langle \mathbf{A} \rangle = \frac{1}{n_s} \int d\mathbf{c}_s f_s \mathbf{A}. \quad (2.6)$$

If we multiply Equation (2.3) by 1, $m_s \mathbf{c}_s$, $\frac{1}{2} m_s c_s^2$, $m_s \mathbf{c}_s \mathbf{c}_s$ and $\frac{1}{2} m_s c_s^2 \mathbf{c}_s$ and integrate over velocity space, we obtain, respectively, the continuity, momentum, energy, pressure tensor and heat flow equations for species s :

Continuity

$$\frac{\partial n_s}{\partial t} + \nabla \cdot (n_s \mathbf{u}_s) = \frac{\delta n_s}{\delta t} \quad (2.7a)$$

Momentum

$$n_s m_s \frac{D_s \mathbf{u}_s}{Dt} + \nabla \cdot \mathbf{P}_s - n_s m_s \mathbf{G} - n_s e_s \left(\mathbf{E} + \frac{1}{c} \mathbf{u}_s \times \mathbf{B} \right) = \frac{\delta \mathbf{M}_s}{\delta t} \quad (2.7b)$$

Energy

$$\frac{D_s}{Dt} \left(\frac{3}{2} p_s \right) + \frac{3}{2} p_s (\nabla \cdot \mathbf{u}_s) + \nabla \cdot \mathbf{q}_s + \mathbf{P}_s : \nabla \mathbf{u}_s = \frac{\delta E_s}{\delta t} \quad (2.7c)$$

Pressure tensor

$$\frac{D_s \mathbf{P}_s}{Dt} + \nabla \cdot \mathbf{Q}_s + \mathbf{P}_s (\nabla \cdot \mathbf{u}_s) + \frac{e_s}{m_s c} [\mathbf{B} \times \mathbf{P}_s - \mathbf{P}_s \times \mathbf{B}] + \mathbf{P}_s \cdot \nabla \mathbf{u}_s + (\mathbf{P}_s \cdot \nabla \mathbf{u}_s)^T = \frac{\delta \mathbf{P}_s}{\delta t} \quad (2.7d)$$

Heat flow

$$\begin{aligned}
&\frac{D_s \mathbf{q}_s}{Dt} + \mathbf{q}_s \cdot \nabla \mathbf{u}_s + \mathbf{q}_s (\nabla \cdot \mathbf{u}_s) + \mathbf{Q}_s : \nabla \mathbf{u}_s + \nabla \cdot \boldsymbol{\mu}_s \\
&+ \left[\frac{D_s \mathbf{u}_s}{Dt} - \mathbf{G} - \frac{e_s}{m_s} \left(\mathbf{E} + \frac{1}{c} \mathbf{u}_s \times \mathbf{B} \right) \right] \cdot (\boldsymbol{\tau}_s + \frac{5}{2} p_s \mathbf{I}) - \frac{e_s}{m_s c} \mathbf{q}_s \times \mathbf{B} = \frac{\delta \mathbf{q}_s}{\delta t} \quad (2.7e)
\end{aligned}$$

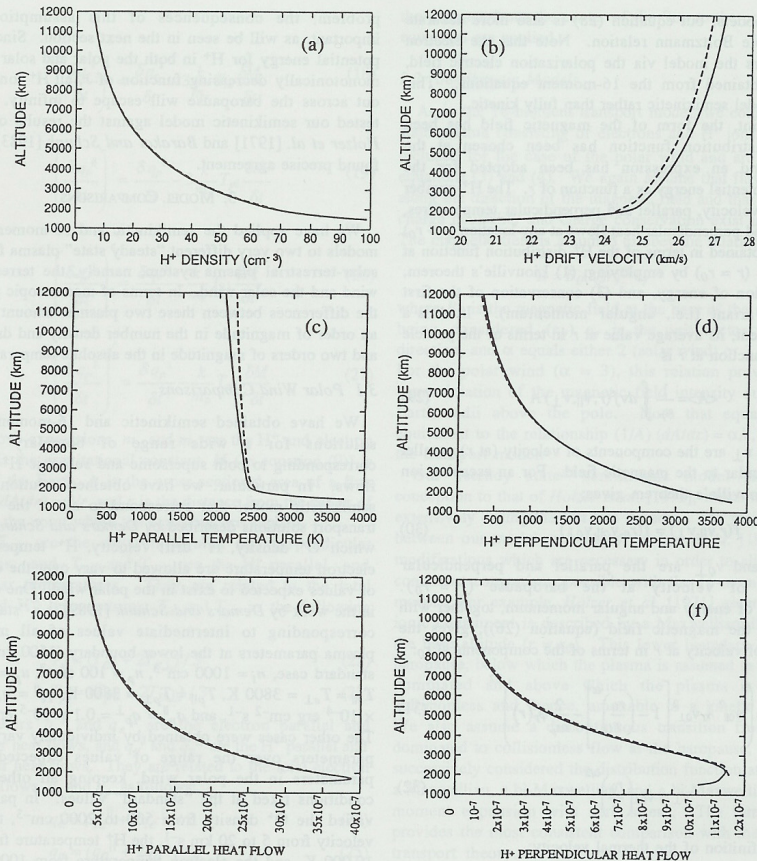
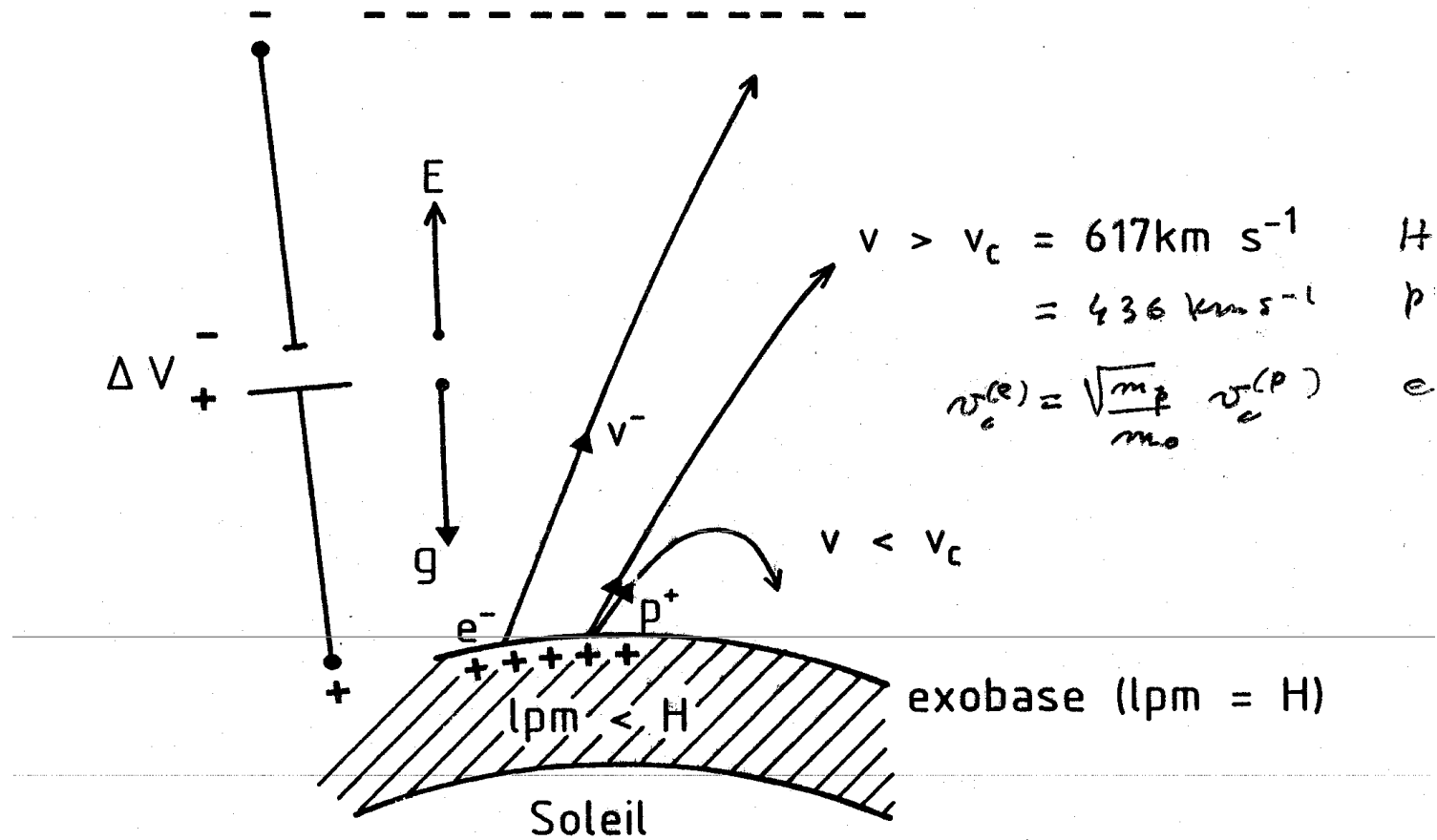


Fig. 1. H⁺ parameter profiles obtained from the semikinetic (dashed curves) and the 16-moment transport (solid curves) models for the supersonic polar wind outflow. Boundary conditions for both models at an altitude of 1500 km (the baropause) are $n(O^+)=1000 \text{ cm}^{-3}$, $n_p=100 \text{ cm}^{-3}$, $u_p=20 \text{ km s}^{-1}$, $T_{p\parallel}=T_{p\perp}=3800 \text{ K}$, and $q_p^\parallel=q_p^\perp=0.1 \times 10^{-5} \text{ erg cm}^{-2} \text{ s}^{-1}$, where the subscript p refers to the H⁺ ions. In addition, the 16-moment transport model assumes that $T_{e\parallel}=T_{e\perp}=3800 \text{ K}$ and $q_e^\parallel=q_e^\perp=-0.11 \times 10^{-4} \text{ erg cm}^{-2} \text{ s}^{-1}$, where the subscript e refers to the electrons. Shown are (a) number density, (b) drift velocity, (c) parallel temperature, (d) perpendicular temperature, (e) parallel heat flow, and (f) perpendicular heat flow. The semikinetic model assumes a 16-moment distribution function with zero stress at 1500 km. (Adapted from Demars and Schunk [1991b].)



Escape velocities for PR electrostatic potential

If $\Delta\Phi_E = - (m_p - m_e) \Delta\Phi_g / 2 e$ (Pannekoek – Rosseland potential)

... the critical escape energy is the same for protons and electrons

$$\frac{1}{2} m_p v_{o,p}^2 = G M_S (m_p + m_e) / 2 r_o = kT \lambda_o = \frac{1}{2} m_e v_{o,e}^2$$

... when electron and proton temperatures are equal ($T_e = T_p$)

$$\lambda_{o,p} = \frac{1}{2} m_p v_{o,p}^2 / kT_p = \frac{1}{2} m_e v_{o,e}^2 / kT_e = \lambda_{o,e}$$

The zero electric current condition [$F_{J,e} = F_{J,p}$] determines
the total electrostatic potential difference :

$$\Delta\Phi_E (> 600 \text{ Volts})$$

This actual value $\Delta\Phi_E$ is much larger than that corresponding
to the Pannekoek-Rosseland potential (150 Volts) which was
assumed in Chamberlain's solar breeze exospheric model

This explains why, in this first exospheric model of the corona,
the solar breeze velocity at 1AU was only 20 km/s